LECTURES ON MARINE ACOUSTICS

Volume II. - Part 2. Selected Advanced Topics

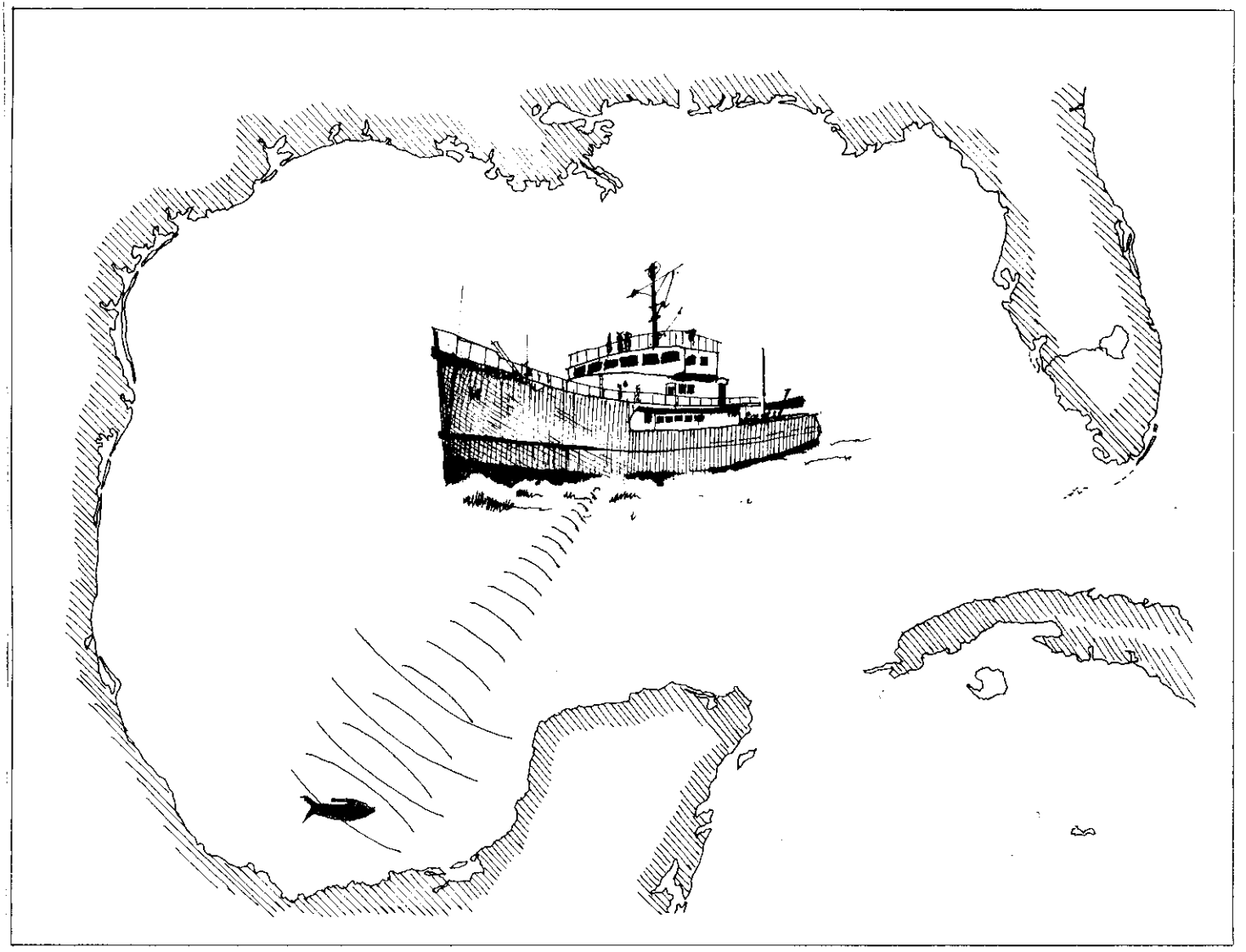

TEXAS A&M UNIVERSITY SEA GRANT PROGRAM

June 1973

TAMU-SG-73-404

LECTURES ON MARINE ACOUSTICS

Lecture notes presented at the 1973 short course
in Marine Acoustics conducted by the
Texas A&M University Department of Oceanography
with partial support of the
National Sea Grant Program
Institutional Grant GH-101 to
Texas A&M University

Volume II - Part II

SELECTED ADVANCED TOPICS IN MARINE ACOUSTICS

April 1973

Sea Grant Publication No. TAMU-SG-73-404

College Station, Texas

FOREWORD

The two volumes LECTURES ON MARINE ACOUSTICS represent compilations of lectures presented at the short course in Marine Acoustics held at the Department of Oceanography of Texas A&M University between June 28 and July 2, 1971. The short course was conducted under the auspices of the National Sea Grant Program of the National Oceanic and Atmospheric Administration, U.S. Department of Commerce, through Institutional Grant GH-101 made to Texas A&M University.

Volume I, *Fundamentals of Marine Acoustics,* is a set of lecture notes prepared for the course "Marine Acoustics" given by the Department of Oceanography on a regular basis. Volume II, *Selected Advanced Topics in Marine Acoustics,* is a compilation of lecture notes presented by invited lecturers. The special lectures that were presented at the course and compiled into Volume II were selected on the basis of their emphasis on the environmental aspect and their application to civil uses.

I am grateful to each author for making his paper ready for reproduction.

Jerald W. Caruthers

FOREWORD TO REVISED EDITION

A second short course in Marine Acoustics was presented at Texas A&M University between June 25 and 29, 1973. Revised editions of LECTURES ON MARINE ACOUSTICS, Volume I, *Fundamentals of Marine Acoustics* and Volume II, *Selected Advanced Topics in Marine Acoustics*, were published for the course. In addition a new set of notes, Volume II - Part 2, *Selected Advanced Topics in Marine Acoustics*, was compiled from the new lectures presented at that time.

Jerald W. Caruthers
June 1973

TABLE OF CONTENTS

NONLINEAR ACOUSTICS WITH APPLICATIONS TO UNDERWATER SOUND

T.G. Muir
Applied Research Laboratories
The University of Texas at Austin
Austin, Texas 78712

Over the past few years, nonlinear acoustics has become more and more important in the fields of both physical and engineering acoustics. Much attention is now being given to practical applications of nonlinear acoustics. The term "nonlinear sonar" has found its way into our vocabulary. Certain nonlinear phenomena have been identified in sonars previously considered to be "linear." As our understanding of nonlinear wave propagation develops with continued research we may see the application of this discipline to technologies other than sonar. The problem of the sonic boom is one example of such an application that is already well developed. The radiation of high intensity noise from jet engines is also of promising interest in this field.

Although nonlinear effects are relatively new to most underwater acousticians, nonlinear acoustics is actually quite an old subject. The history of this discipline has been documented[1] and it is evident that nonlinear acoustics was an important topic in the evolution of classical physics. This work dates back to Euler (1755) and features such master practicioners as Lagrange, Poisson, Stokes, Airy, Earnshaw, Riemann, and Rayleigh, who concentrated on the propagation of plane waves in lossless gasses. Recent work has been facilitated by modern sonar technology, especially by the development of high intensity sound sources. At present, the main thrust of new developments in nonlinear acoustics comes from underwater sound.

In the treatment to follow, we will be limited to a modern interpretation of nonlinear effects in underwater sound. The problems of finite amplitude distortion, shock formation, and saturation will be described. The topic of parametric arrays will also be treated as it is perhaps the most significant nonlinear effect in sonar applications.

The experiments presented to illustrate the theory were conducted by the author at Applied Research Laboratories' Lake Travis Test Station. It should be stated that many excellent experiments have been conducted by others and that their omission was made for reasons of convenience only. Finally, theory and experiment are separated for the purpose of allowing those not well founded in mathematics to proceed with the more easily understood experimental section.

THEORY

Since it will be necessary to refer to several theoretical developments in the evolution of nonlinear acoustics that may not be widely appreciated, it is convenient to review some of the more important concepts that are fundamental to the subject matter.

The Equations of Fluid Mechanics

For lossless media, the three equations of fluid mechanics that form the basis of acoustics are those of continuity, conservation of momentum, and the physical equilibrium or state of the medium. These equations may be stated mathematically as follows.

Continuity equation

$$\frac{\partial \rho_T}{\partial t} + \nabla \cdot (\rho_T \vec{u}) = 0 \quad , \tag{1}$$

Momentum equation

$$\frac{\partial}{\partial t}(\rho_T \vec{u}) + \rho_T \vec{u}(\nabla \cdot \vec{u}) + (\vec{u} \cdot \nabla)\rho_T \vec{u} + \nabla p = 0 \quad , \tag{2}$$

Isentropic equation of state

$$p = \sum_{n=1}^{\infty} \frac{1}{n!} \left(\frac{\partial^n p}{\partial \rho^n} \right)_{\rho=\rho_o, S} \rho^n \quad , \tag{3}$$

where

$\rho_T = \rho_o + \rho$, total density,

ρ_o = static or equilibrium density,

ρ = excess density,

∇ = the vector differential operator,

$\vec{u}$ = particle velocity,

t = time,

p = acoustic or excess pressure,

n = a summation index, and

S = entropy.

The equation of state shown here is a Maclaurin series expansion of the pressure-density relation. It is usually approximated by retaining only the first two terms in the series, i.e.,

$$p = c_o^2 \rho + \frac{1}{2} \frac{c_o^2}{\rho_o} \left(\frac{B}{A}\right) \rho^2 \quad , \tag{4}$$

where

$$c_o^2 = \left(\frac{\partial p}{\partial \rho}\right)_{\rho=\rho_o, S} \quad , \tag{5}$$

and

$$\frac{B}{A} = \frac{\rho_o}{c_o^2} \left(\frac{\partial^2 p}{\partial \rho^2}\right)_{\rho=\rho_o, S} \quad . \tag{6}$$

Equation (5) is the definition of the small signal sound speed, c_o, whereas Eq. (6) may be taken as the definition of the "parameter of nonlinearity" of the medium, following the nomenclature of Beyer.[2] The results of several measurements indicate that B/A has the value 5.2 for degassed fresh water at 30°C.[2] If the medium is a gas (rather than a liquid), the equation of state is usually given by the adiabatic law,

$$\frac{p_T}{p_o} = \left(\frac{\rho_T}{\rho_o}\right)^{\gamma} \quad , \tag{7}$$

where

γ = the ratio of the principal specific heats, and

p_o = the static pressure.

By application of the binomial expansion to Eq. (7), one can show the equivalence of Eqs. (3) and (7). Moreover, if γ is replaced by $1 + B/A$, the two results are identical, through second order. This will allow the development of a second-order theory for liquids which can be applied to gases through the transformation

$$\frac{B}{A} = \gamma - 1 \quad .$$

Since the emphasis of this lecture is on underwater sound the derivations will employ the equation of state given by Eq. (4).

Distortion and Shock Formation

A classic problem in nonlinear acoustics is the distortion and formation of shocks in large amplitude waves. This process has also been shown to have a great influence on high amplitude parametric arrays.

The underlying cause of finite amplitude distortion is the dependence of the signal speed on the particle velocity. (The signal speed is defined as the velocity of any specified point on an acoustic waveform.) This dependence may be obtained from the basic equations of fluid mechanics, but it is sufficient to state it here as*

$$\frac{dx}{dt} = c_o + \left(1 + \frac{1}{2}\frac{B}{A}\right)u \quad , \tag{8}$$

where

$\frac{dx}{dt}$ = the signal speed, and

u = the particle velocity.

Because the particle velocity varies with location on the waveform, points on the waveform in a condensed phase travel faster than those in a rarefaction phase. If the original wave has a sinusoidal shape, this variation in signal speed will cause a cumulative distortion in the wave shape as the wave travels, until a shock forms. The various stages in this process are demonstrated by the waveforms shown in Fig. 1. For spherical waves, the range at which a shock forms is given by

$$\bar{r} = r_o \exp\left(\frac{1}{\beta\epsilon k r_o}\right) \quad , \tag{9}$$

where

$\beta = \left[1 + \frac{1}{2}\frac{B}{A}\right]$

$\epsilon = \frac{u_{max}}{c_o}$, the acoustic Mach number,

$k = \frac{2\pi}{\lambda}$, the wave number, and

r_o = the radius of the spherical source, or the range at which spherical divergence begins.

*The evolution of this result has been documented in ref. 1.

INITIAL WAVEFORM
($r = r_0$, $\sigma = 0$)

SHOCK FORMATION
($r = \bar{r}$, $\sigma = 1$)

MATURE SAWTOOTH
($r = \bar{r}$, $\sigma = 3$)

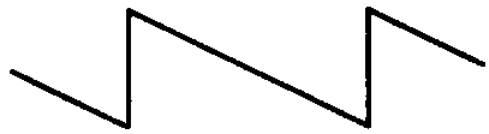

OLD AGE
($r >> r_{max}$)

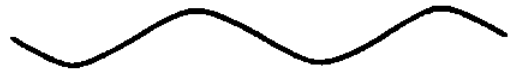

FIGURE 1
FINITE AMPLITUDE WAVEFORMS

ARL - UT
AS-70-1497
TGM - RFO
11 - 17 - 70

The process of shock formation is often characterized in terms of a dimensionless parameter σ, defined (for spherical waves) as

$$\sigma = \beta\epsilon k r_o \ln \frac{r}{r_o} \quad . \tag{10}$$

The initial formation of a vertical discontinuity takes place when $\sigma=1$, as is shown in Fig. 1. At this point, the fundamental frequency component of the waveform suffers about 1 dB of attenuation due to the process of distortion, as will be demonstrated in
If the amplitude of the initial waveform is high enough to cause further distortion, a sawtooth waveform may be obtained at a range $\tilde{r}$ corresponding to $\sigma=3$, i.e.,

$$\tilde{r} = r_o \exp\left(\frac{3}{\beta\epsilon k r_o}\right) \quad . \tag{11}$$

At this point, the distortion and the dissipation at the shock front can cause several decibels of attenuation of the fundamental, depending on the role that ordinary dissipation plays in the problem at hand.

Since multivalued waveforms are physically impossible, the tendency for further distortion must be matched by dissipation at the shock front. In this sense, the sawtooth waveform is a stable waveform because it maintains its shape until the dissipation finally reduces its amplitude to a level commensurate with small signal acoustics.

The transition range between finite amplitude and small signal regions can be obtained by equating the rates of the two types of dissipation. For spherical waves, this range is given by

$$r_{max}^{(n)} = \frac{\beta\epsilon k r_o}{\alpha_n\left[1+\beta\epsilon k r_o \ln\left(\frac{r_{max}}{r_o}\right)\right]} \quad , \tag{12}$$

where α_n = the small signal attenuation coefficient for the nth harmonic.

Finite-Amplitude Propagation and Saturation

For relatively strong waves at ranges shorter than r_{max}, weak shock theory (which is based on perturbation solutions of Eqs. (1) through (3)) can be taken as a reasonably valid method for the analysis of finite amplitude waveforms. Of prime importance is the problem of describing the behavior of the frequency components in a train of originally sinusoidal waves. Blackstock[3] obtained a general solution of this problem through a Fourier series expansion of certain solutions resulting from weak shock theory that describe the time-domain behavior of the waveforms. For spherical waves, this expansion may be stated as,

$$p = p_o\left(\frac{r_o}{r}\right)\sum_{n=1}^{\infty} B_n \sin n[\omega t - k(r-r_o)] \quad , \tag{13}$$

where

$$B_n = \left(\frac{2}{n\pi}\right) W_b + \frac{2}{n\pi\sigma}\int_{\Phi_{min}}^{\pi} \cos n\,(\Phi - \sigma \sin \Phi)\,d\Phi \quad ,$$

$$W_b = \left(\frac{1}{\sigma}\right)\left[j_o^{-1}\left(\frac{1}{\sigma}\right)\right]U(\sigma-1) \quad ,$$

$j_o^{-1}\left(\frac{1}{\sigma}\right)$ = the quantity whose zero-order spherical Bessel function is $\frac{1}{\sigma}$, and

$$\Phi_{min} = \sigma W_b \quad .$$

The B_n's in this solution are the Fourier coefficients of the harmonic components of the distorted waveform.

As was stated above, Eq. (13) is strictly valid for ranges $r<r_{max}$. Its validity at greater ranges may be approximated[4,5] by allowing B_n to take on the form

$$B_n' = \left[1 - U\left(r-r_{max}^{(n)}\right)\right] B_n + \left[U\left(r-r_{max}^{(n)}\right)\right] B_n\left(r=r_{max}^{(n)}\right) e^{-\alpha\left(r-r_{max}^{(n)}\right)} \quad .$$

In this approximation, B_n is assumed to represent the only absorption agency out to the $r_{max}^{(n)}$ range. At this range, the B_n damping factor is switched out by the step function, $1 - U\ r-r_{max}^{(n)}$, and small signal absorption takes over, beginning with the amplitudes specified by the value of B_n at $r=r_{max}^{(n)}$.

An important consequence of Eq. (13) and its corollaries is the concept of acoustic saturation. By allowing the amplitude at the source to increase indefinitely, it can be shown[4] that the amplitude at the fundamental frequency approaches a finite, limiting value. The result is

$$p_{(sat)}^{1} = \frac{2\rho_o c_o^2}{\beta k r \ell n \left(r_{max}^{(1)_\infty} / r_o \right)} \exp\left[-\alpha_1 \left(r - r_{max}^{(1)_\infty} \right) \right] \quad , \tag{14}$$

where

$$r_{max}^{(1)_\infty} = \int_{p_o \to \infty} r_{max}^{(1)} = \left[\alpha_1 \ell n \left(r_{max}^{(1)_\infty} / r_o \right) \right]^{-1} \quad .$$

An interesting feature of Eq. (14) is that it does not depend on the amplitude at the source. Equation (14) can also be interpreted as saying that the medium refuses to sustain and propagate arbitrarily intense sounds and that a limiting value will always be reached, above which more intense sounds are impossible. Note also that the presence of α_1 in the negative exponential and k in the denominator of Eq. (14) serves to reduce the saturation level with increase in frequency. At very low frequencies, saturation is unlikely.

Harmonic Generation

As one might suspect, the nonlinear distortion experienced by a propagating finite amplitude wave results in the generation of harmonic components. As the waveform becomes steeper and steeper, more and more harmonics are generated. Equation (13) can be used to predict the frequency spectra of the harmonic components as a function of range. Two particularly simple and perhaps useful features of the harmonic radiations can also be extracted from Eq. (13). The first has to do with the relative amplitudes of harmonic components. In the sawtooth region, these amplitudes are related to the amplitude of the fundamental through the factor 1/n. This means that the maximum relative amplitude of the second harmonic is 6 dB below the fundamental, while the third harmonic is 10 dB down, the fourth harmonic 12 dB, etc. Although absorption reduces the harmonic amplitudes at ranges associated with $r_{max}^{(n)}$, especially in the old age region, they nonetheless have fairly respectable amplitudes in the sawtooth region. The second feature provided by the theory summarized in Eq. (13) is that each successive harmonic has a progressively smaller beam, with progressively greater minor lobe suppression. Prior to shock formation, for example, the directivity function of the nth harmonic goes as the directivity of the fundamental to the nth power; i.e., for $\sigma_1 < 1$,

$$D_n(\theta) = [D_1(\theta)]^n \tag{15}$$

In the sawtooth region, where $\sigma_1 > 3$ and $r < r_{max}^{(n)}$, the directivities go as

$$D_n(\theta) = D_1(\theta) \frac{1 + \sigma_1}{1 + \sigma_1 D_1(\theta)} \quad . \tag{16}$$

In the sawtooth case, the harmonic beamwidths and minor lobe levels are greater than for the preshock case, although there is a marked decrease in these parameters with increase in harmonic number.

The fact that the harmonic radiations exist at respectable levels in high intensity transmissions (at times regardless of the intent of the designer), coupled with the fact that they can be highly directive, makes their utility in high resolution applications quite attractive.

Parametric Arrays

In 1960, P. J. Westervelt[7] at Brown University developed the theory for a sound source that he called a parametric acoustic array. This type of source allows for the creation of highly directive sound at relatively low operating frequencies through the nonlinear interaction of acoustic waves. The original theory treated the problem of the interaction of two plane, collimated, monochromatic carrier waves emitted simultaneously from a high frequency projector. A sketch of the geometry is shown in Fig. 2(a). The carrier waves were shown to interact nonlinearly in the medium within a zone of modulation that is bounded by the collimated beam and extends a distance along the acoustic axis determined by the small signal absorption of the carrier waves. In this sense, the parametric acoustic array may be thought of as a volumetric end-fired array that occupies a portion of the medium directly in front of the projector.

The engineering significance of the parametric array is due to its great directivity, specifically its narrow beamwidth and the absence of minor lobes in its radiation patterns. The narrow beamwidth is a result of the shape of the zone of modulation. By analogy to the ordinary end-fired array, it can be easily seen that the longer the zone of modulation, the smaller is the beamwidth of the parametric array. Since the zone of modulation is usually very long in comparison to its width, the parametric array produces a radiation much narrower than that which would be produced by the source transducer were it operating linearly at the difference frequency. The parametric array is shaded by virtue of the naturally smooth decay in the conversion of carrier frequency sound to difference frequency sound with increasing distance from the electroacoustic source. This inherent form of array shading, which is due to the absorption of the carrier waves, and to diffraction within the zone of interaction, gives rise to an angular response that decays monotonically with increasing angle from the acoustic axis. In other words, the beam pattern of the parametric array contains none of the undesirable minor lobe structures common to conventional piston type transducers.

Although the generation of difference frequency sound is of the greatest current interest, it should be pointed out that parametric arrays also generate sound at frequencies equal to the sum of the original primary frequencies.

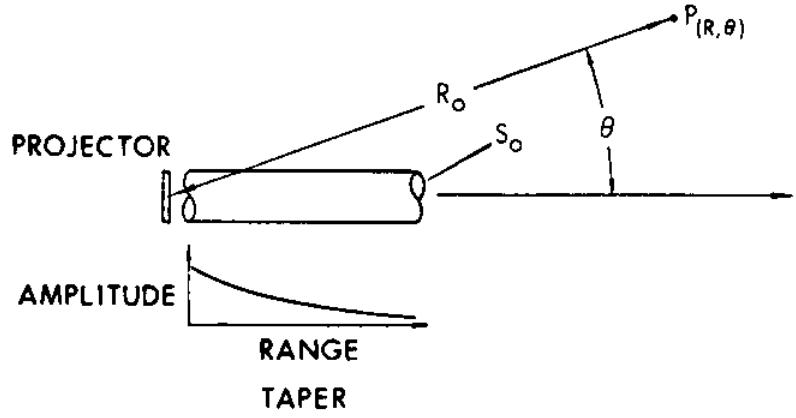

(a) PARAMETRIC TRANSMITTER, GEOMETRY
FOR THE ASYMPTOTIC, PLANE WAVE SOLUTION

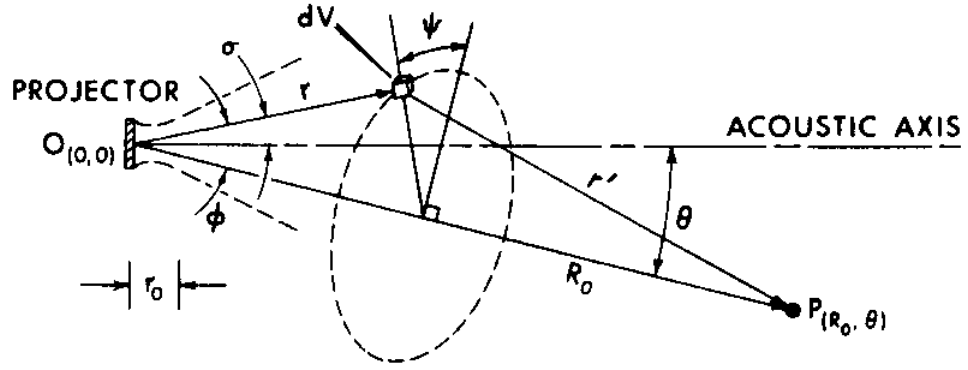

(b) PARAMETRIC TRANSMITTER, GEOMETRY
FOR THE NUMERICAL SPHERICAL WAVE SOLUTION

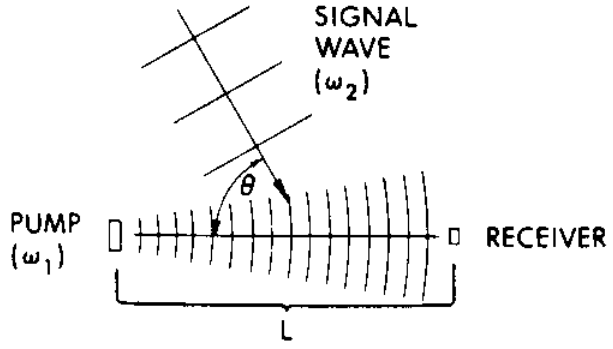

(c) PARAMETRIC RECEIVER, GEOMETRY
FOR THE SPHERICAL WAVE SOLUTION

FIGURE 2
PARAMETRIC ACOUSTIC ARRAYS

ARL - UT
BS-73-319
TGM DR
4-18-73

The theory underlying the parametric array problem has its roots in the basic Eqs. (1) through (3), as do the other problems previously discussed. In working with these equations, Westervelt found an inhomogeneous wave equation appropriate for the description of parametric interaction. This is

$$\square p_s = - \frac{\beta}{\rho_o c_o^4} \frac{\partial}{\partial t^2} p^2 \quad , \tag{17}$$

where

$\square$ is the d'Alembertian operator, $= \Delta^2 - 1/c_o^2 \, \partial^2/\partial t^2$,

p_s is the sum of the two carrier amplitudes, and

p_s is the amplitude of difference frequency sound.

The solution of Eq. (17) for the geometry of Fig. 1(a) is

$$p_s(R_o,\theta) = \frac{\beta \omega_s^2 p_1 p_2 S_o}{8\pi R_o \rho_o c_o^4} \frac{1}{\left[\alpha^2 + k_s^2 \sin^4(\theta/2)\right]^{1/2}} \quad , \tag{18}$$

where

α is the mean carrier or primary wave attenuation coefficient,

S_o is the cross-sectional area of the primary beam,

p_1 and p_2 represent the primary wave amplitudes, and

the subscript s indicates difference frequency parameters.

The half-power beamwidth of the difference frequency radiation can be obtained from Eq. (18) as

$$\theta_{HP} = 4\sqrt{\frac{\alpha}{k_s}} \quad . \tag{19}$$

Equation (19) can be used to show that the beamwidth is reduced by reducing the primary frequencies and increasing the difference frequency. Experimental evidence of the general validity of Eqs. (18) and (19) was first reported in 1963 by Bellin and Beyer[8] and has continued to appear[9-17] since that time.

Refinements to the solution represented by Eq. (18) have also been made. One of these[18] is of practical significance in underwater sound as it allows the extension of theory to spherical wave propagation in the farfield of the primary electroacoustic source(s). This modification also allows for an exact description of the primary wave directivities of these sources. For a circular piston projector, as shown in Fig. 2(b), the result may be stated as

$$p_s(R_o,\theta) = \frac{2p_1p_2r_o^2\omega_s^2\beta}{\Pi\rho_o c_o^4 k_1 k_2 a^2} \int_{r_o}^{R_o} \int_{o}^{\phi_e+\theta} \int_{o}^{\Pi}$$

$$\cdot \frac{J_1\left(k_1 a \sin\sigma(\psi,\phi,\theta)\right) J_1\left(k_2 a \sin\sigma(\psi,\phi,\theta)\right)}{\sin^2\sigma(\psi,\phi,\theta)} \qquad (20)$$

$$\cdot \frac{\exp -\left\{\left[(\alpha_1+\alpha_2) - ik_s\right] r - (ik_s-\alpha_s)r'(r,\phi)\right\}}{r'(r,\phi)} \sin\phi d\psi d\phi dr \quad ,$$

where, as a result of some elementary trigonometry,

$$\sin\sigma(\psi,\phi,\theta) = \left\{[\sin(\theta-\phi) + \sin\phi\,\cos\theta(1-\cos\psi)]^2 + \sin^2\phi\,\sin^2\psi\right\}^{1/2} \quad ,$$

and

$$r'(r,\phi) = \left(R_o^2+r^2-2rR_o\,\cos\phi\right)^{1/2} \quad .$$

In this solution, $J_1(\cdot)$ is the first order Bessel function of argument $(\cdot)$ and ϕ_e is taken to be some effective angle which covers the main concentration of energy in the primary beam. The subscript "s" also describes the generation of sum frequency sound in this solution, depending on the assignment of quantities. All other symbols not defined by the geometry of Fig. 2(b) are as defined for previous solutions. The closed-form solution of Eq. (20) has not yet been found so that at present one must use numerical integration techniques in order to treat practical problems. These techniques are nonetheless very straightforward and many computations have been made with Eq. (20) showing good agreement with experiment.

Parametric Reception

The receiver analogy of the parametric transmitter was recognized[7] early in the development of parametric arrays, and was shown to exist shortly thereafter.[10] The basic concept is illustrated in Fig. 2(c). An incoming signal at some low frequency ω_2 is made to interact with a high intensity "pump" wave of frequency ω_1, where $\omega_1 > \omega_2$. The receiver is tuned to the side band(s) containing the interaction frequency(s).

The theory of parametric receivers has been developed by Berktay,[19] who solved Eq. (17) for several boundary conditions. The result of one such derivation, for the sum and difference frequency pressure amplitudes at a point a distance L in the farfield of the pump transducer (on its acoustic axis), is given in the form

$$p_s(L,\theta) = - \frac{(\omega_1 \pm \omega_2)\beta P_1 P_2}{2\rho_o c_o^3} \exp\{-(\alpha_s + jk_s)L \mp jM\} D(\theta) \quad , \qquad (21)$$

where

$$D(\theta) = \frac{\sin M}{M}$$

and

$$M = k_2 L\,(1-\cos\theta)/2 \quad .$$

The result is valid for L much greater than the nearfield distance of the pump transducer, and for those situations in which the pump beamwidth is less than that of an end-fired array of length L and frequency ω_2. Some significant features of this result should be pointed out.

1) The solution is independent of the directivity function of the pump transducer.
2) The directivity function of the parametric receiver is independent of the pump frequency, and is the same whether the sum or the difference frequency component is used.
3) The axial response of the parametric receiver is dependent on its length L only through the absorption term.

In general, parametric reception offers a means to develop directive receivers at low frequencies with small transducers. The beamwidth of such a system is equivalent to that of a linear end-fired array of length L. In the parametric receiver, however, only two transducer elements are required, while the linear end-fired array usually requires a large number of elements distributed over its length.

EXPERIMENTS

Since the theoretical results of the previous section predict some rather remarkable effects that are of increasing importance in practical applications of underwater sound, it is appropriate to illustrate these results by comparison to experiment. A number of measurements have been made in fresh water with a 3 in. diam piston[4,5] projector, operating at a fundamental frequency of 450 kHz. The transmitting apparatus consisted of an oscillator, gate, and power amplifier, and the receiver was made up of the usual components common to transducer calibration work.

Saturation Measurements

We begin with some simple measurements on the system at high power. Data for the amplitude response on the acoustic axis, with range as a parameter, is presented in Fig. 3. The input-output curves shown were each measured as a function of input power at six different range stations. The ordinate labeled "extrapolated peak source level" was obtained from linear theory and was verified by the linearity of data taken at the shortest range, 0.76 yd. Since only the range was changed for each successive curve, it is clear that nonlinearly induced losses in the medium are responsible for the progressive roll-off from linearity. The theoretical saturation levels are shown as horizontal line segments on the right of the figure. Since the saturation formula was obtained by letting p_o approach infinity, and since the experimental values for this parameter were finite, one should not expect exact agreement between predicted and measured levels. The discrepancy at the three longest ranges, where plateaus in the response curves are best approached, is nonetheless only a few decibels. The approximate nature of Eq. (14), coupled with the fact that no account of nearfield distortion was made in the present calculations, renders this comparison of theory and experiment quite satisfying. Nearfield distortion is evident in the amplitude response data at the shortest range, 0.76 yd, but in the calculations, a pure sinusoid was assumed at the minimum range r_o=0.9 yd, which is half the Rayleigh distance for the projector used. The spherical theory presented in the previous sections should be reasonably accurate since most of the distortion occurred in the farfield of the projector. Proper accounting of nearfield distortion should close the gap between theory and experiment, and is therefore a subject worthy of further examination.

The progressive roll-off from linearity in the input-output curves of Fig. 3 demonstrates an important practical consequence of nonlinear effects in high intensity transmissions. As saturation is approached, one quickly arrives at a region of diminishing return, where, for example, a 1 dB increase in source level may effect only a fraction of a decibel increase in SPL at the field point. In this region, further increase in the size of the power amplifier is practically useless.

Finite Amplitude Propagation of the Fundamental Component

The propagation of spherical waves under the influence of nonlinear effects leading to and including saturation is also of importance in

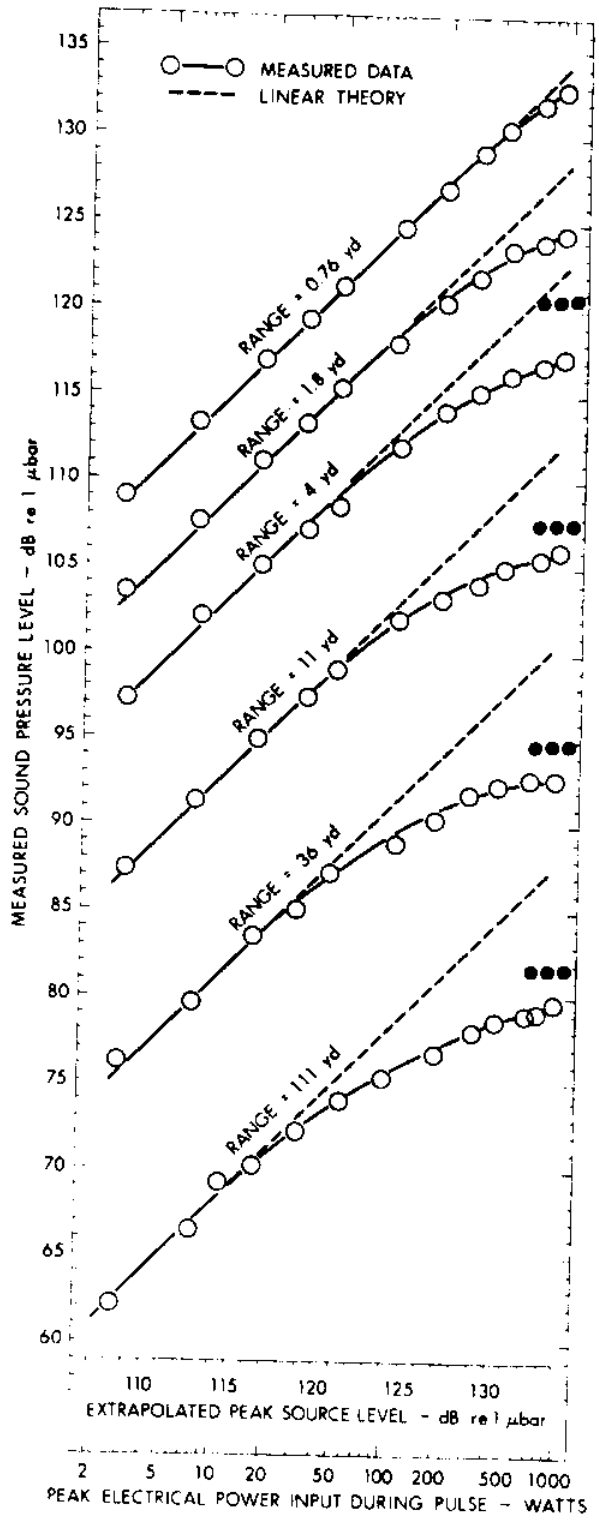

FIGURE 3
AMPLITUDE RESPONSE CURVES SHOWING THE EFFECT OF EXTRA LOSSES CAUSED BY NONLINEAR EFFECTS
(3 in. diam PISTON PROJECTOR, f = 454 kHz, DI = 36.5 dB, η = 40%)

understanding the consequences of finite amplitude attenuation. Propagation data, abstracted from the amplitude response curves of Fig. 3 for six different levels of transmitted power, is shown in Fig. 4. Here, the solid lines indicate the results of computations with Eq. (13) and its corollaries. The dashed lines represent the approximate extension of farfield theory to the nearfield. The blank space in the propagation curves signifies that the 111 yd data were taken at a different time of the year than the other data, when the water was warmer and was therefore slightly less absorptive. Again, satisfactory agreement between theory and experiment was obtained.

The influence of nonlinear effects can be seen in the separation of the curves. At low amplitudes, there is as much separation at the shorter ranges as there is at long ranges. At high amplitudes, however, the separation diminishes with increase in range, demonstrating an amplitude-dependent attenuation. The decrease in the separation of these curves again demonstrates the diminishing return effect; that is, one obtains just about as much SPL at the long ranges by transmitting at a source level of 130 dB as is obtained by transmitting at a source level of 134 dB. This occurs despite the fact that the transmitted power is increased by a factor of 2.5.

Beam Patterns of the Fundamental Component

Mutations in the beam patterns of nonlinearly influenced radiations were observed in the present experiments, as they were in previous experiments in air.[6] This phenomenon is illustrated by the measured data presented in Fig. 5, which shows a pair of beam patterns of the 454 kHz piston at each of the six range stations used. The high amplitude patterns, taken at a peak source level of 133 dB re 1 μbar at 1 yd, are shown in Fig. 5(a), while the low amplitude patterns, taken at a 1 yd source level of 115 dB are shown in Fig. 5(b). The first patterns, taken at a range of 0.76 yd, show the effect of a measurement in the nearfield of the projector in that the minor lobe structures are not yet fully developed. The onset of the minor lobe is nonetheless about 1 dB higher in the high amplitude pattern as compared to its low amplitude counterpart. The width of the major lobe is also slightly larger in the high amplitude pattern. This trend continues with increase in range as is evident in the remaining five beam pattern pairs. At the maximum range, an 80% increase in the half-power beamwidth results and the minor lobe suppression decreases by 7 dB. These effects may be explained by noting that the major lobe is in the domain of nonlinear acoustics and hence suffers finite amplitude attenuation, while the minor lobes are of sufficiently low amplitude to be well approximated by linear theory and to suffer little or no extra attenuation.

Since in many sonar applications it is desired to operate with as narrow a beam and as good a minor lobe suppression as possible, beam broadening and loss of suppression due to nonlinear effects can degrade sonar operation as much or even more than the loss in amplitude previously described.

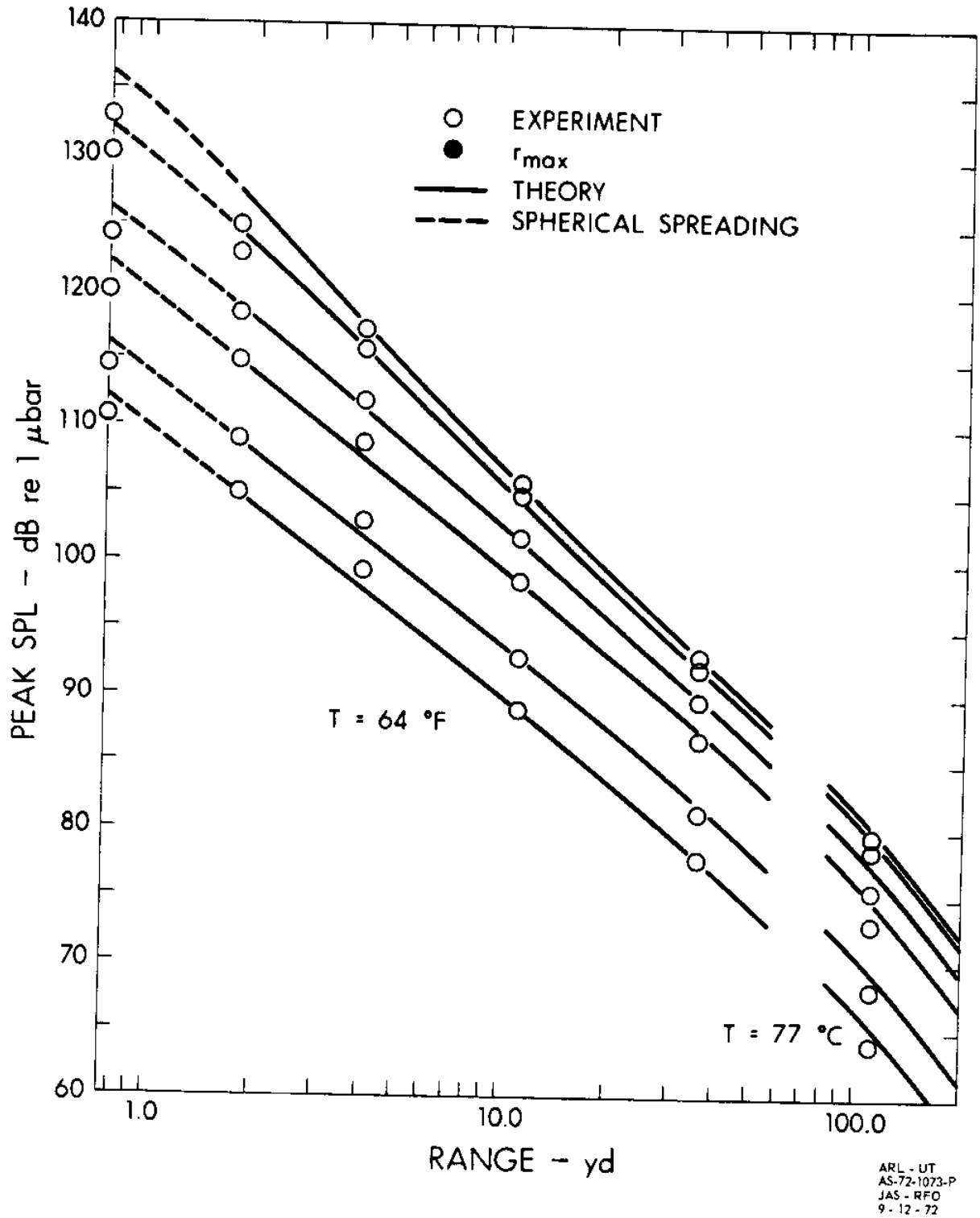

FIGURE 4
PROPAGATION CURVES

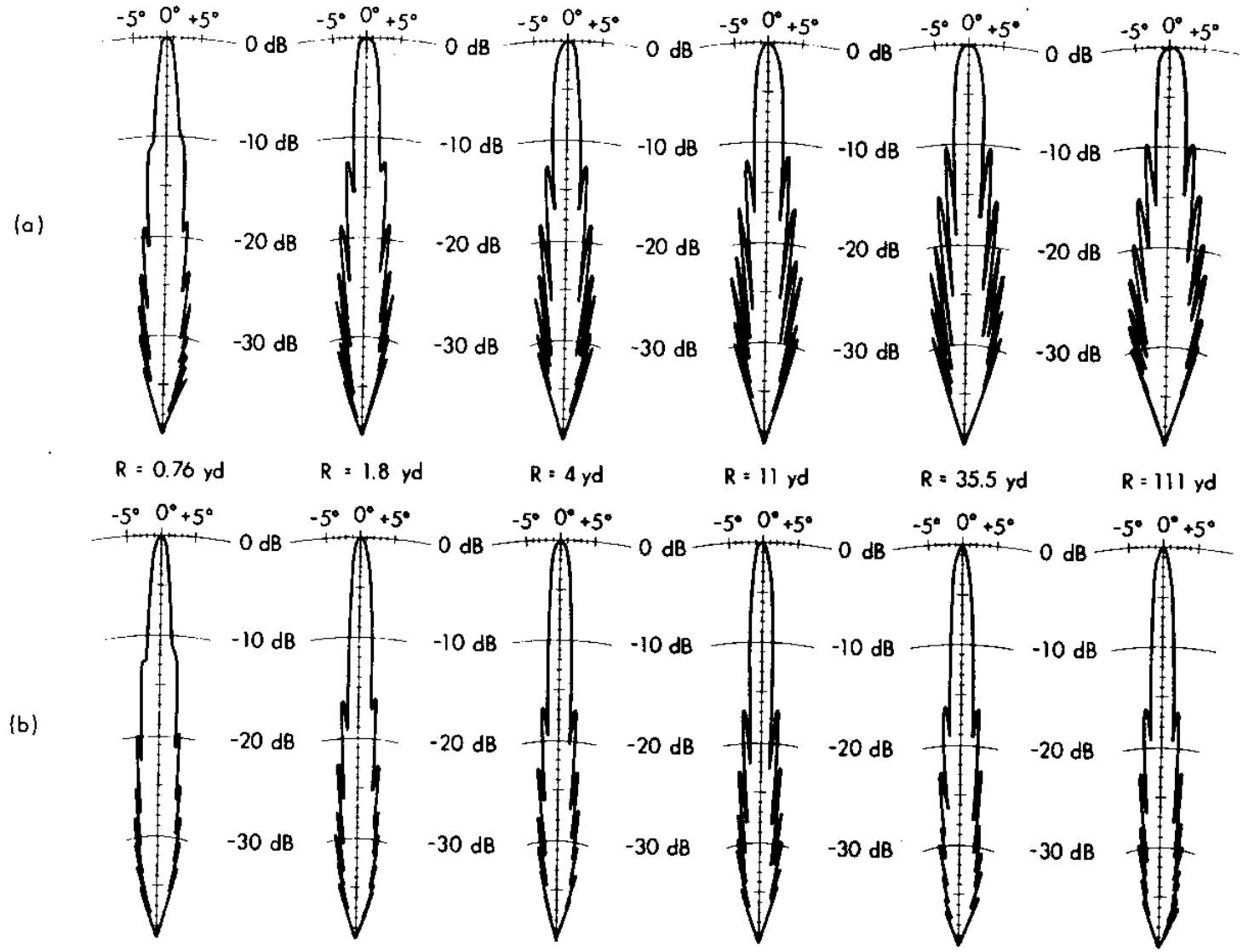

FIGURE 5
BEAM PATTERNS AT VARIOUS RANGES FOR A STRONG AND A WEAK WAVE
(3 in. diam PISTON PROJECTOR, f = 454 kHz, DI = 36.5 dB, η = 40%)

Propagation of Harmonic Radiations

The propagation of harmonic components in a finite amplitude wave having a source level of 127 dB re 1 μbar at 1 yd is illustrated in Fig. 6. As can be seen, the harmonics exist and their amplitudes are surprisingly high, even though this source level-frequency combination was not sufficient to generate a mature sawtooth wave. The theory summarized by Eq. (13) is quite accurate at the shorter ranges and lower harmonic numbers, and fairly accurate elsewhere.

Beam Patterns of the Harmonic Radiations

Directivity measurements made in conjunction with the above described propagation data are shown compared to theory in Fig. 7. As can be seen, there is a progressive reduction in beamwidth with increase in harmonic number. This occurs despite the fact that there was some beam broadening due to saturation effects. The minor lobe levels are also reduced with increase in harmonic number. Each of these trends is most desirable in high resolution sonar. The utilization of harmonic radiations in underwater acoustics should therefore be recognized as a potentially useful technique. It should be pointed out that operation at preshock levels (i.e., those for which Eq. (15) is valid) provides for much higher directivity than demonstrated by the example presented here.

Parametric Array Propagation Curves

Experiments with parametric arrays may be conducted in several ways. One of these is to sum the outputs of two oscillators in a linear adder and then apply the amplified combination signal to a single, linear projector. Another method involves the use of two sets of interleaved transmitting arrays in which each array is allocated a single carrier frequency. The former method was used[18] to obtain the data shown in Fig. 8. For these measurements, each carrier was transmitted at a peak source level of 108 dB re 1 μbar, referred to a range of 1 yd. The axial propagation data for a carrier radiation at a mean frequency of 450 kHz and for the sum and difference frequency radiations are shown compared to theory. The curve for the mean carrier was constructed from nearfield theory for the axial response, and includes spreading and absorption in the farfield. Although both the sum and difference frequency radiations undergo spreading, they experience a noticeable influx of energy, out to a range of 50 to 100 yd, where the difference frequency curve is seen to asymptotically approach the spherical spreading curve. The sum frequency curve appears to approach the spreading curve sooner, but this is due primarily to the high absorption at this frequency. The sum frequency data show a considerably higher amplitude than the difference frequency data. This can be explained on the basis of the dependence of amplitude on the square of the frequency as given in Eq. (20). As mentioned earlier, Eq. (20) is valid only for interaction in the farfield of the carrier transducer. The theoretical curves shown in Fig. 8 were computed with the nearfield parameter $r_o=3a^2/4\lambda_c$. This choice for the nearfield-farfield "boundary" was based on the realization of the farfield half-power beamwidth at this range. The fact that most

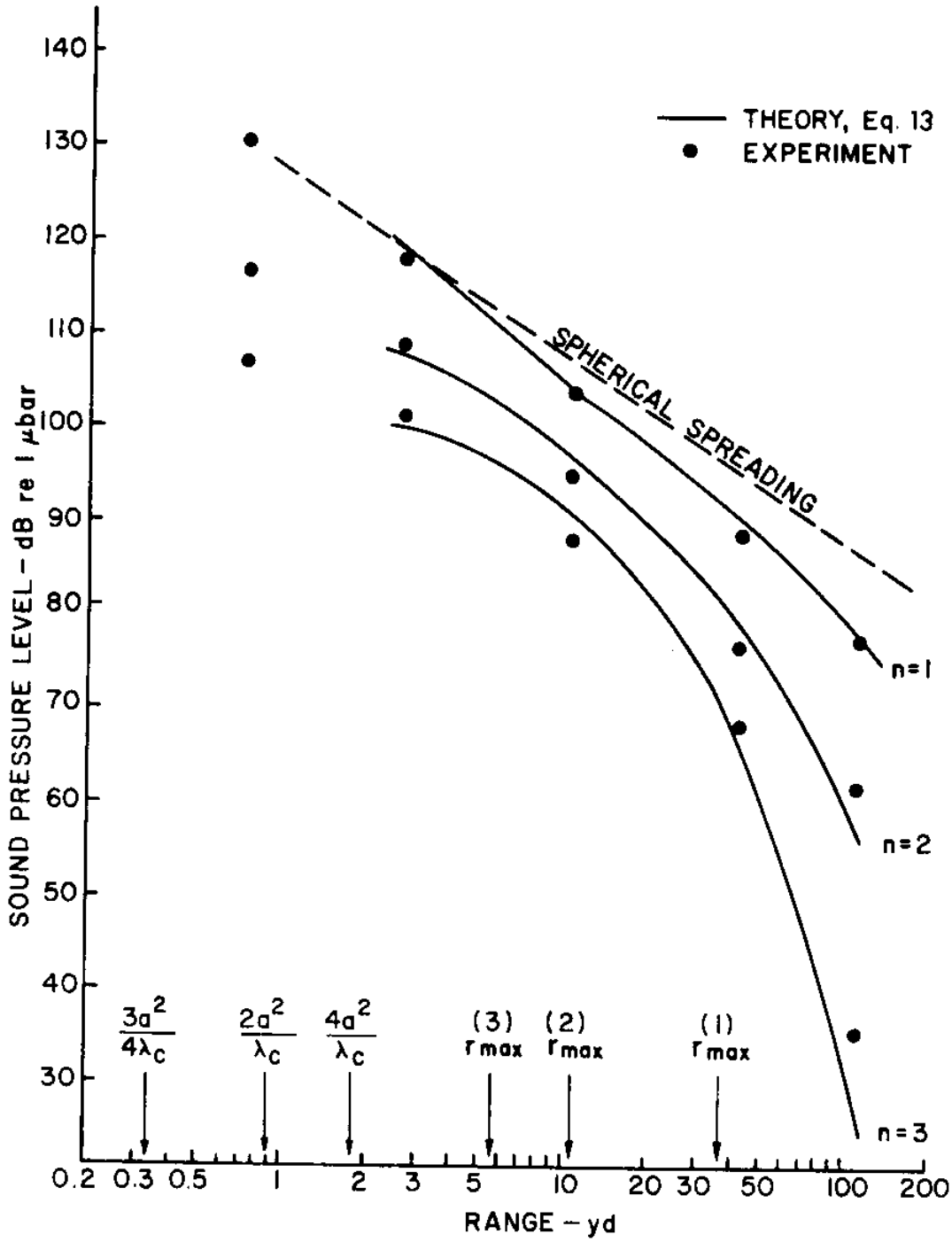

FIGURE 6
PROPAGATION CURVE
HARMONICS IN A SPHERICAL WAVE OF FINITE AMPLITUDE

ARL - UT
AS-71-595
TGM - RFC
5 - 26 - 71

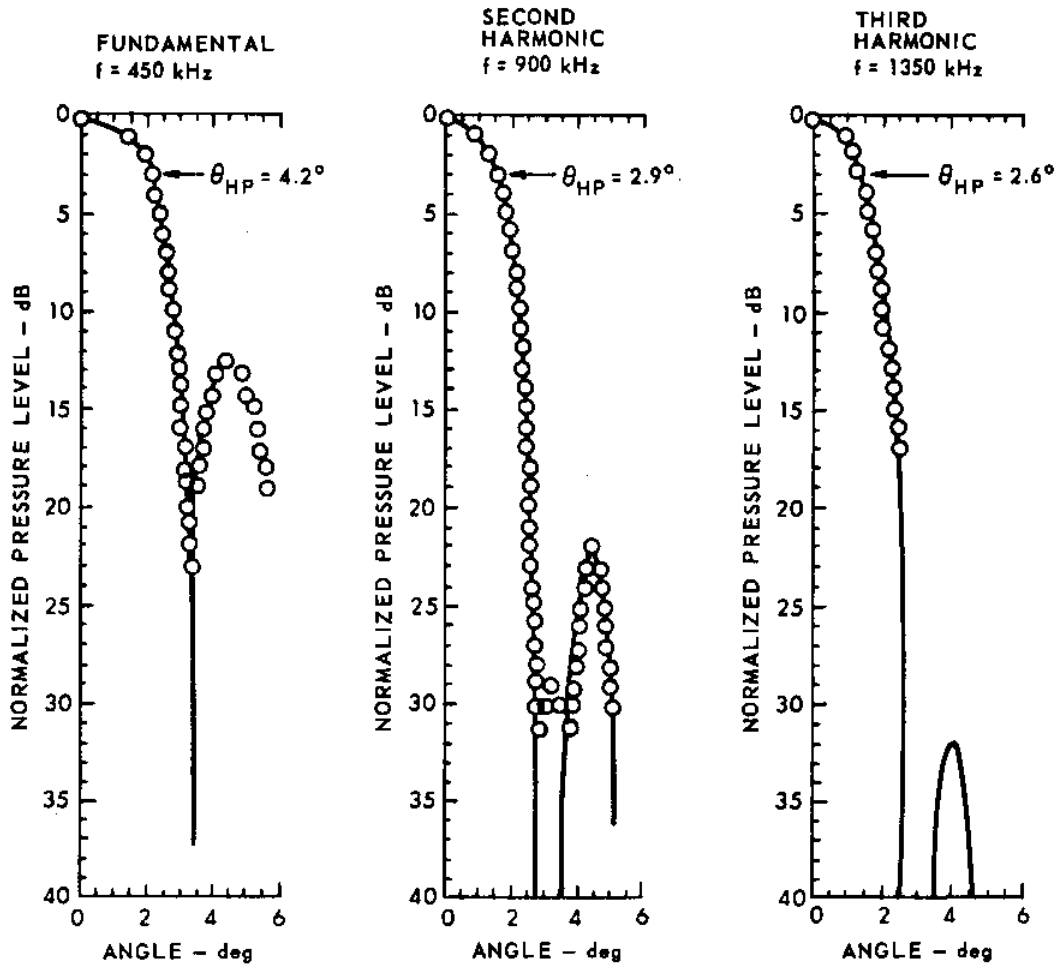

FIGURE 7
BEAM PATTERN DATA FOR STRONG WAVES
ooo EXPERIMENT —— THEORY
FUNDAMENTAL SOURCE LEVEL = 127 dB re 1 μbar at 1 yd
PATTERNS MEASURED AT R = 112 yd

ARL - UT
AS-71-343-S
TGM - DR
3 - 22 - 71

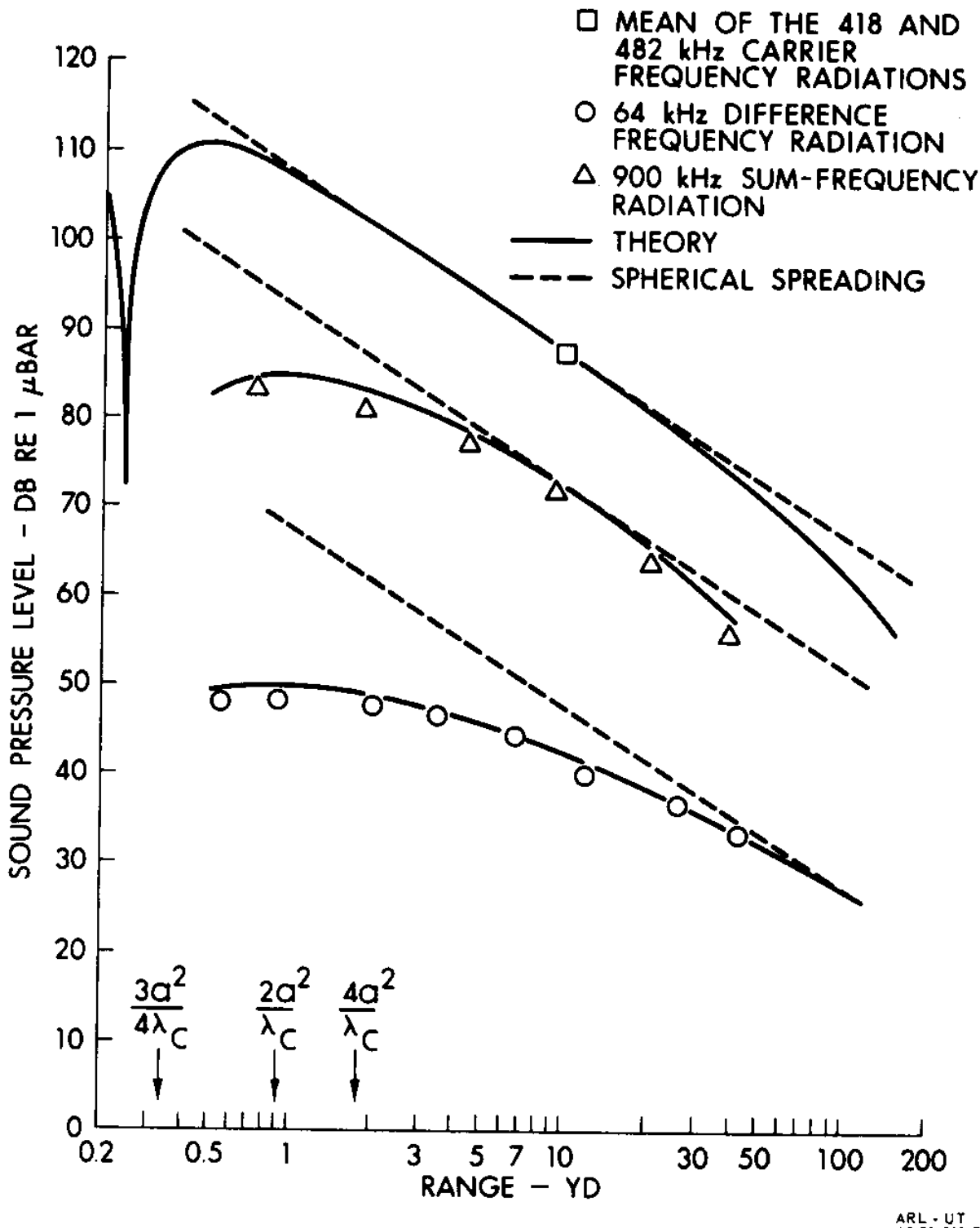

FIGURE 8
PARAMETRIC ARRAY PROPAGATION CURVES

of the nonlinear interaction took place in the farfield of the present experiment did not make the choice of r_o particularly critical, at least for ranges $R_o >> r_o$. The agreement between theory and experiment shown in Fig. 8 is within experimental error.

The relative amplitudes of the data shown in Fig. 8 indicate that the parametric conversion process is an inefficient one. This is indeed the case, as efficiencies on the order of 1% are common. It can be shown, however, that the parametric efficiency is directly proportional to the primary power, provided shocks are not formed in the carrier waves. In considering practical applications of parametric arrays, the reduction of primary transducer size must be weighed against the inefficiency of the process. As will be shown subsequently, the wide band nature of the parametric process enables one to recapture much of the conversion loss by use of wide band signal processing techniques.

Parametric Array Beam Patterns

Directivity measurements of the two carriers and of the difference frequency radiation are shown in Fig. 9. The carrier patterns demonstrate the usual minor lobe structures common to linear transducers, while the difference frequency pattern is devoid of minor lobes, in accordance with theory. The narrow width of the difference frequency beam is also evident. For the parameters of the experiment at hand, the difference frequency beamwidth is practically the same as either carrier. Had a linear radiation at a frequency equal to the difference frequency been radiated from the projector linearly, the resulting beamwidth would have been about 8 times larger. This demonstrates the practical utility of parametric arrays in providing high resolution sound beams with small apertures.

The beam patterns of sum frequency parametric arrays are practically identical to those for the second harmonic radiations, due primarily to their similarity in frequency.[18]

Bandwidth of Parametric Arrays

As was mentioned earlier, the parametric interaction process is somewhat inefficient. One way to overcome this inefficiency is to utilize the wide bandwidth character of parametric conversion. This feature is illustrated in Fig. 10, which shows photographs and frequency spectra for the principal waveforms in a parametric array experiment involving cw pulses. The double peak in the carrier spectra indicate a concentration of energy at the two main carrier frequencies, with some energy in the side band lobes. The width between nulls in the main carrier bands is 4 kHz, for the experiment at hand. The width between nulls of the main difference frequency band is also 4 kHz. This indicates a bandwidth translation from carrier to difference frequency sound that enables the generation of extremely wide band radiations at low frequencies. It is a simple matter, for example, to obtain a 15% bandwidth with an ordinary high frequency electroacoustic source. Use of a carrier band centered at, say, 100 kHz would then lead to a 15 kHz difference frequency band centered at 7.5 kHz. Other possibilities exist.[19] Many of the well known wide band signal processing techniques (such as replica correlation, etc.) can then be used to extract the parametric signals from background noise.

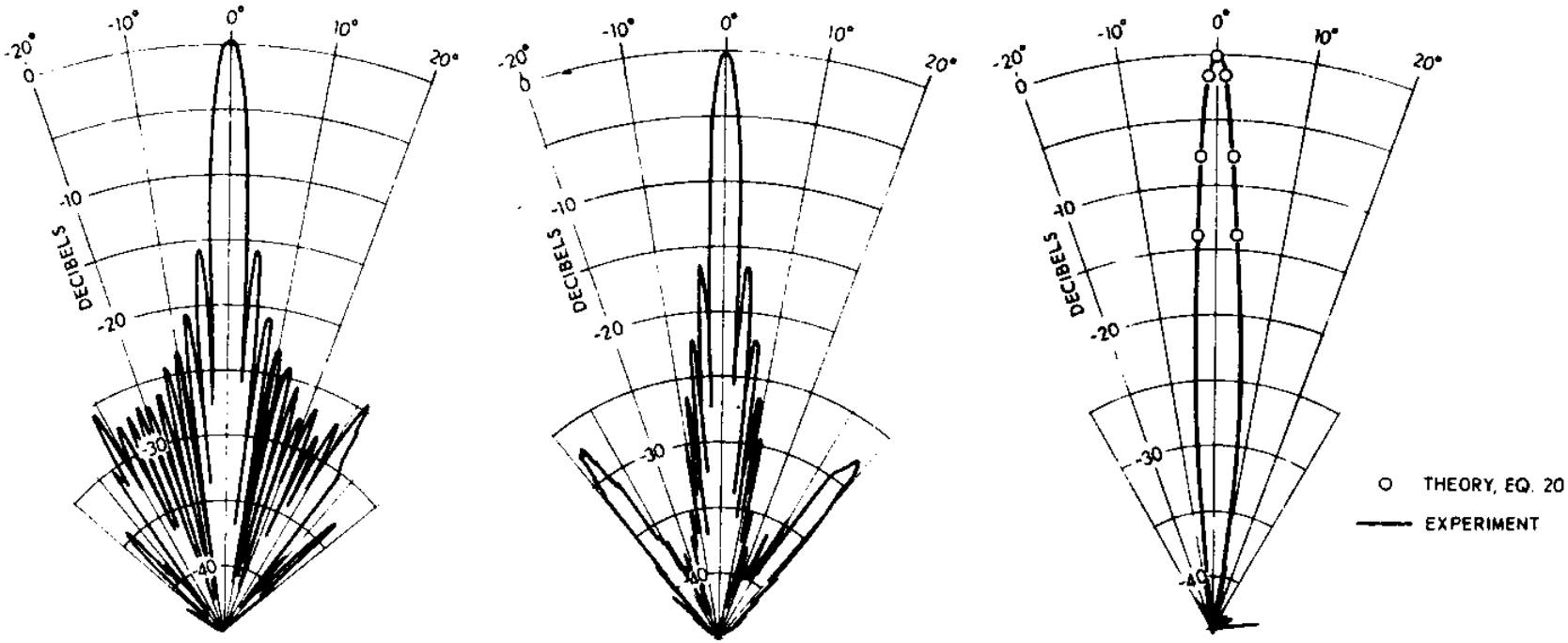

BEAM PATTERN OF THE 418 kHz CARRIER

BEAM PATTERN OF THE 482 kHz CARRIER

DIFFERENCE-FREQUENCY BEAM PATTERN

FIGURE 9
PARAMETRIC TRANSMITTING
ARRAY DIRECTIVITY PATTERNS

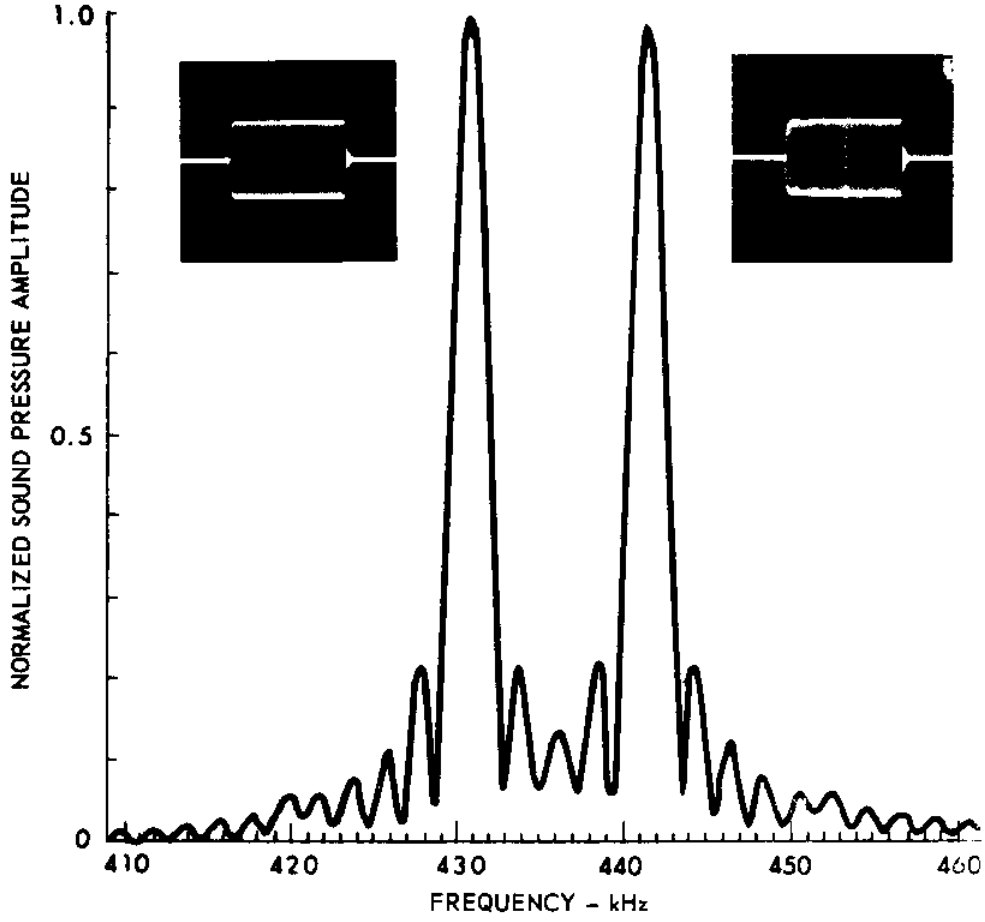

PULSE SHAPE AND FOURIER SPECTRUM OF THE CARRIERS

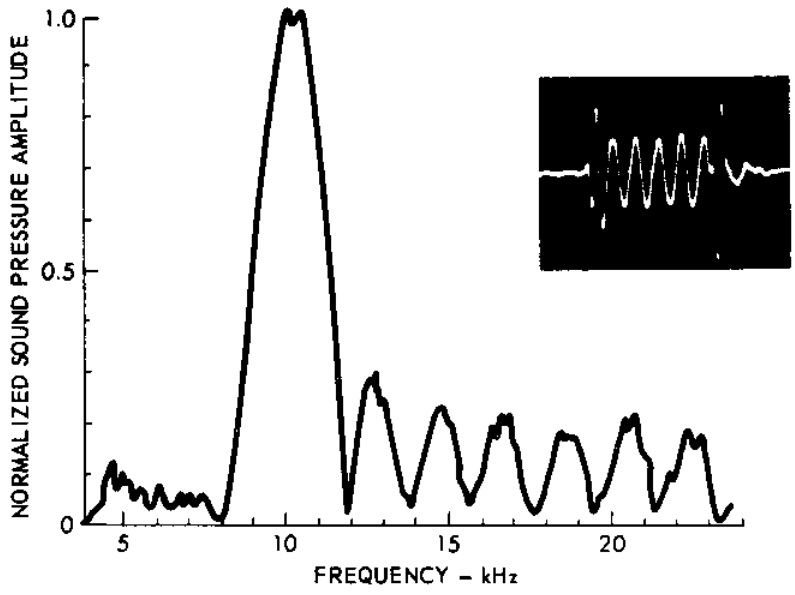

FIGURE 10

PULSE SHAPE AND FOURIER SPECTRUM OF
DIFFERENCE FREQUENCY SOUND

ARL - UT
BS-72-1000
TGM - RFO
8 - 22 - 72

The "spikes" on the leading and trailing edge of the difference frequency pulse of Fig. 10 are due to a nonlinear transient effect associated with the interaction of side band energy. (See, for example, Ref. 20.)

Parametric Receiving Array Beam Patterns

Several recent measurements have been conducted with parametric receiving arrays having parameters as shown in Fig. 11. The pump(s) and receiver(s) were suspended from horizontal booms that were rotated so as to enable the acquisition of the beam pattern data shown. The pattern in part (a) of the figure was taken with a single parametric receiver composed of a pump projector that was 1 in. in diameter, and a hydrophone 1/2 in. in diameter. The 460 kHz pump frequency signal was rejected by a crystal filter, leaving only the 455 kHz difference frequency signal. The signal wave had a level of 70 dB re 1 μbar at the center of the array whereas the pump source level was 96 dB re 1 μbar at 1 yd. The interaction component had a level of +28 dB re 1 μbar at the receiver. The pattern obtained was somewhat narrower than predicted by Eq. (21).

In practice, one would utilize a more intense pump level than used here, since the amplitude of the low frequency signal wave would be expected to be much lower. A good choice for pump frequencies is the band from 40 to 100 kHz, where sea state and thermal noise are minimized. At present, the operation of the parametric receiver is thought to involve the translation of the signal and its associated noise band to the band containing the pump frequency. If so, the original signal-to-noise ratio is preserved (provided the noise in the pump band is low) and enhanced by the directivity gain of the parametric receiver itself.

It is possible to combine pump-receiver combinations, i.e., parametric receiving elements, in arrays of parametric arrays to perform any number of array functions.[21] Data resulting from the combination of four such elements, identical to the one described above, is shown in part (b) of Fig. 11. Here, the use of four parametric receivers to form a broadside array has effected a sizeable reduction in beamwidth, in accordance with ordinary array theory. This type of array can also be steered electrically by inserting a progressive phase shift in the output of each element. The data shown in part (c) of Fig. 11 demonstrate this technique of beam deflection, showing two beams separated by a steered angle of 6°. Since the steered sector is limited by the width of the single element pattern, the length of each parametric end-fired receiver need not be inconveniently large.

In order to shed some light on the potential advantages of arrays of parametric receivers, some comparisons to equivalent linear systems should be made. First, consider a 4-element linear system having roughly the same transducer area as the 4-element parametric receiver just described. Unlike the parametric system, the linear system would possess grating lobes of equal sensitivity at $\theta=30°$ and 90°, and there would be no discrimination against signals or noise arriving from both the back of

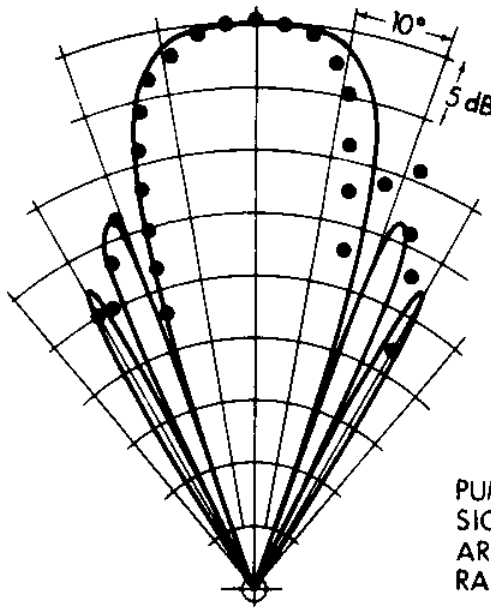

PUMP: 460 kHz
SIGNAL: 5 kHz
ARRAY LENGTH: 19 ft
RANGE: 127 yd

(a) SINGLE ELEMENT PARAMETRIC RECEIVER

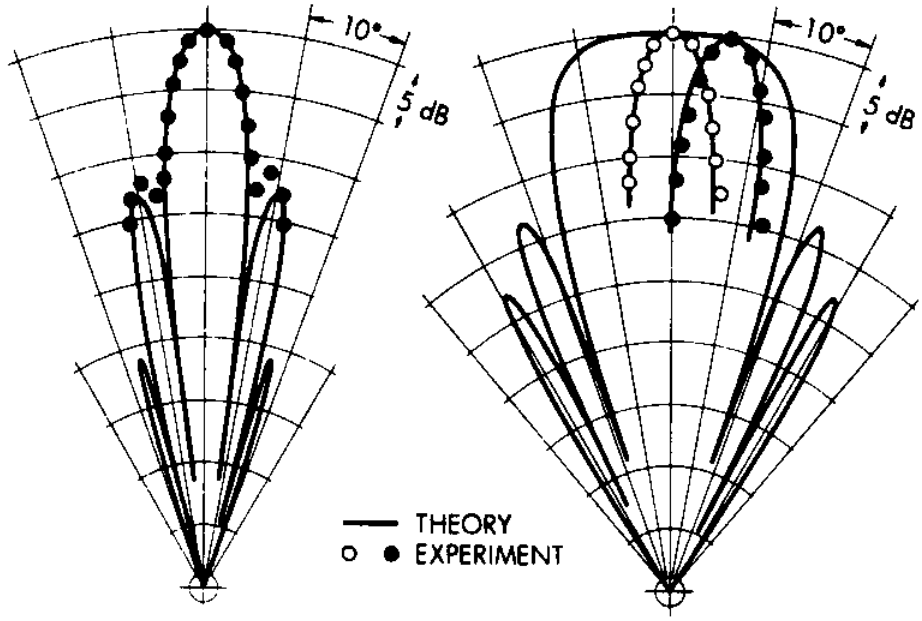

(b) 4-ELEMENT ARRAY OF PARAMETRIC RECEIVERS

(c) BEAM STEERING OF 4-ELEMENT ARRAY

FIGURE 11
PARAMETRIC RECEIVING ARRAY MEASUREMENTS

ARL - UT
BS-73-320
TGM - DR
4 - 18 -

the array and from angles contained in the vertical plane. Next, consider a 4-element linear system with the same acoustic properties as the aforementioned parametric system. This would require four piston transducers whose largest dimension would be 2.5 ft, which amounts to a surface area of 2820 sq in., or roughly 720 times that of the parametric device.

It should not be implied that transducer size and cost are the only factors to be considered in the comparison of linear and parametric systems. Clearly, the electronics associated with active arrays of the parametric type are more complex than those associated with passive arrays. However, the increased electronic complexity need not be prohibitive if the proper choice of parameters is made.

REFERENCES

1. D. T. Blackstock, "History of Nonlinear Acoustics and a Survey of Burgers' and Related Equations," in Nonlinear Acoustics, Proceedings of the 1969 ARL Symposium, T. G. Muir, Ed. (1970).

2. R. T. Beyer, "Parameter of Nonlinearity in Fluids," J. Acoust. Soc. Amer. 32, 719 (1960).

3. D. T. Blackstock, "Connection Between the Fay and Fubini Solutions for Plane Sound Waves of Finite Amplitude," J. Acoust. Soc Amer. 39, 1019 (1966).

4. J. A. Shooter, T. G. Muir, and D. T. Blackstock, J. Acoust. Soc. Amer. 49, 119(A) (1971); to be published as "Acoustic Saturation of Spherical Waves in Water," (1973).

5. J. C. Lockwood, T. G. Muir, and D. T. Blackstock, J. Acoust. Soc. Amer. 50, 124(A) (1971); to be published as "Directive Harmonic Generation in the Radiation Field of a Circular Piston," (1973).

6. C. H. Allen, "Finite Amplitude Distortion in a Spherically Diverging Sound Wave in Air," Ph.D. Theses, Pennsylvania State University (1950).

7. P. J. Westervelt, "Parametric Acoustic Array," J. Acoust. Soc. Amer. 35, 535-537 (1963).

8. J. L. S. Bellin and R. T. Beyer, "Experimental Investigation of an End-Fire Array," J. Acoust. Soc. Amer. 34, 1051-1054 (1962).

9. H. O. Berktay, "Possible Exploitation of Nonlinear Acoustics in Underwater Transmitting Applications," J. Sound. Vib. 2, 435-461 (1965).

10. H. O. Berktay, "Parametric Amplification by the Use of Acoustic Nonlinearities and Some Possible Applications," J. Sound. Vib. 2, 462-470 (1965).

11. H. O. Berktay, "Some Proposals for Underwater Transmitting Applications of Nonlinear Acoustics," J. Sound. Vib. 6, 244-254 (1967).

12. V. A. Zverev and A. I. Kalachev, "Measurement of the Scattering of Sound by Sound in the Superposition of Parallel Beams," Sov. Phys. Acoust. 14, 173-178 (1968).

13. H. O. Berktay, "Nonlinear Interactions between Acoustic Waves in Liquids--Possible Applications," Application of Finite Amplitude Acoustics to Underwater Sound, Proceedings of a Seminar held at the U. S. Navy Underwater Sound Laboratory on 27 May 1968, NUSL Rpt. No. 1084, 15-38 (1970).

14. T. G. Muir and J. E. Blue, "Acoustic Modulation of Large Amplitude Waves," J. Acoust. Soc. Amer. 46, 227-232 (1969).

15. D. G. Tucker, "A Review of Progress in Underwater Acoustics," Radio and Elec. Engrs., U.D.C. 621-39, 69-84 (1970).

16. R. H. Mellen, D. G. Browning, and W. L. Konrad, "Parametric Sonar Transmitting Array Measurements," to be published

17. See, for example, Nonlinear Acoustics, Proceedings of the 1969 ARL Symposium, T. G. Muir, Ed., Applied Research Laboratories, The University of Texas at Austin (1970).

18. T. G. Muir and J. G. Willette, "Parametric Acoustics Transmitting Arrays," J. Acoust. Soc. Amer. 52, 1481-1486 (1972).

19. See, for example, H. O. Berktay and J. A. Shooter, "Parametric Receiver with Spherically Spreading Pump Waves," J. Acoust. Soc. Amer. 53

20. T. G. Muir and J. E. Blue, "Transient Response of the Parametric Acoustic Array," in Nonlinear Acoustics, Proceedings of the 1969 ARL Symposium, T. G. Muir, Ed., Applied Research Laboratories, The University of Texas at Austin.

21. H. O. Berktay and T. G. Muir, "Arrays of Parametric Receiving Arrays," scheduled for publication, J. Acoust. Soc. Amer., May (1973).

Ivor D. Groves, Jr.
Standards Branch
Underwater Sound Reference Division
Naval Research Laboratory

INTRODUCTION

The science of underwater acoustics is a relatively new field compared to some. Most of the discoveries and the understanding of this field have been found or developed since World War I. It is claimed that the natives of ancient Ceylon signaled each other at sea by striking a submerged earthen vessel to produce a sharp percussive click that could be heard miles away by an ear held against the bottom of a boat. Even as far back as 1490 a device is shown in one of the notebooks of Leonardo de Vinci for detecting sounds underwater. It consisted of a hollow tube pressed to the ear with the other end extending into the water. While the ear is a very sensitive device, it is not a calibrated instrument that can accurately measure the sound pressure at any particular point. Although some people can accurately determine the frequency of a sine wave, few, if any, claim that they can accurately ($\pm$1.0 dB) determine the sound pressure level by ear.

In underwater acoustic measurements, calibrated hydrophones are usually used to determine the sound pressure level (SPL). This level may be expressed in decibels using any of several reference pressure levels.

$$SPL = 20 \log \frac{p_1}{p_o}$$

where p_o is a reference pressure.

There is no universally accepted standard reference pressure; however, in accordance with "American National Standard Preferred Reference Quantities for Acoustical Levels, S1.8-1969" most underwater acoustic measurements made today by Naval activities and all such calibration measurements made at the Naval Research Laboratory, Underwater Sound Reference Division, Orlando (NRL-USRD), use the reference pressure level one micronewton per square meter ($\mu N/m^2$), which is called the micropascal (μPa).

The relationship of each of the reference levels is easier to remember if the values shown in Fig. 1 are kept in mind.

If a reference other than the micropascal has been used, such as the microbar, it is easy to change to the new reference by adding +100 dB to obtain the pressure, source level, or transmitting response. You add -100 dB to obtain the receiving sensitivity. Thus a source level of +50 dB re 1 microbar becomes +150 dB re 1 micropascal and a receiving sensitivity of -90 dB re 1 volt/microbar becomes -190 dB re 1 volt/micropascal.

The symbols, such as M for microphone or receiving sensitivity and S for speaker or transmitting response, are not defined in the "American Standard Acoustical Terminology" but are used in "American Standard Procedures for Calibration of Electroacoustic Transducers, Particularly Those for Use in Water, Z24.24-1957." Most of the literature does use these symbols; but here again there are inconsistencies and some publications use S for voltage sensitivity of the hydrophone.

The first requirement for determining an unknown SPL is a calibrated hydrophone where the free-field voltage sensitivity has been expressed as a function of frequency. This is usually obtained by either the comparison or the reciprocity method.

Although there are some special calibration techniques using closed tanks, generally a free-field environment is desired. This is a homogeneous isotropic medium free of boundaries. A perfect free field is never achieved; therefore, it is necessary to know the best procedures to minimize the effects of boundaries, temperature gradients, gas bubbles, and marine life.

Comparison Calibration of Hydrophone in a Free Field

If we consider first the comparison method of calibration we see that it appears to be a relatively simple measurement. In this method the hydrophone being calibrated and the calibrated reference standard hydrophone are subjected to the same free-field sound pressure by placing each hydrophone in turn in the sound field and comparing the electrical output voltages of the two hydrophones. This method also is known as the substitution method, because the unknown is substituted for the standard without otherwise changing the measurement conditions. A typical equipment set-up is shown in Fig. 2 with provision for measuring the current e_i/R in the projector and the voltage e across the projector.

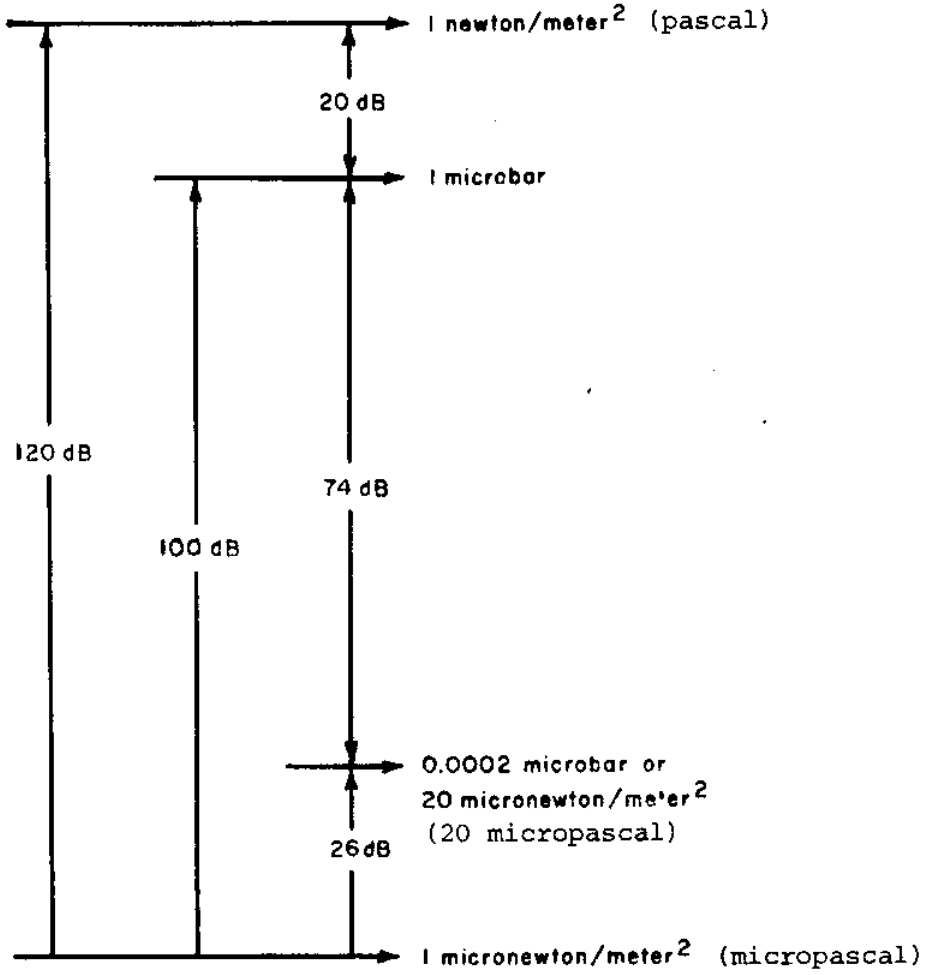

1 newton/meter^2 = 1 pascal (abbreviation: Pa)

1 micronewton/meter^2 = 1 micropascal (abbreviation: μPa)

FIG. 1. Reference pressure levels.

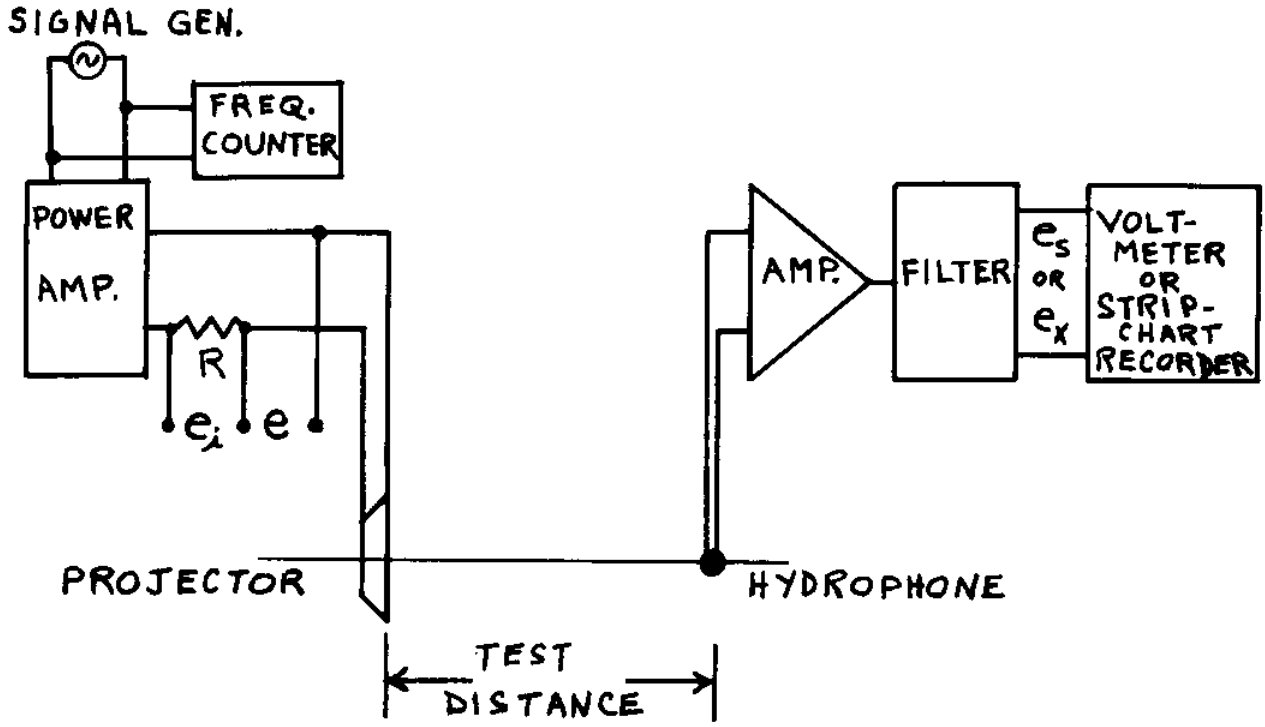

FIG. 2. A typical equipment set-up for calibration measurements.

There are several practical considerations which must be taken into consideration. When the standard hydrophone is immersed in the sound field, it must be far enough from the projector (sound source) that it intercepts a segment of the spherical wave small enough (or having a radius of curvature large enough) that the segment is indistinguishable from a plane wave. Even the preamplifier housing must be taken into consideration because such housings frequently affect the sensitivity.

Unless the standard hydrophone is omnidirectional, it must be oriented so that its acoustic axis points toward the projector. This includes both azimuth and depth. Figure 3 illustrates how we could obtain an inverse effect of distance loss when the measurement is made at two distances, 1 and 2, if the projector and hydrophone acoustic axes are not in alignment at the same depth. This is especially true when the project or hydrophone is not omnidirectional.

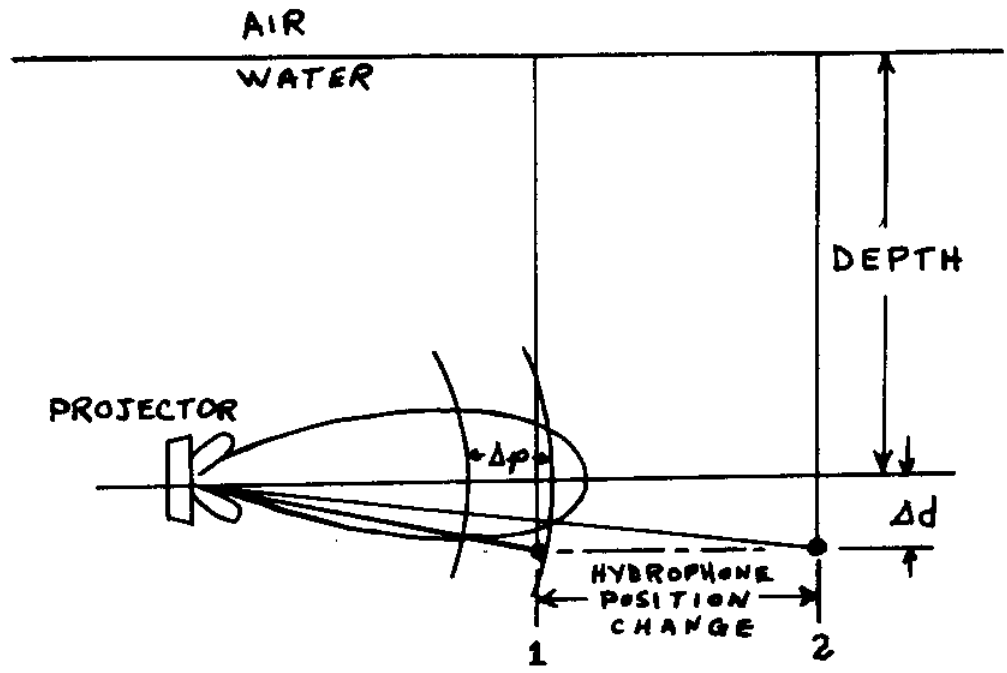

FIG. 3. Inverse distance loss Δp due to depth error Δd.

It is a good practice to make the measurements at two distances both to check alignment of the transducer and to see that a number of other measurement conditions are met.

For example, if the distance is changed from 40 to 50 cm, the distance loss is 20 log (5/4) = 2 dB. If the distance-loss measurement and theory agree, then all of the following conditions are usually satisfied:

1. There is no proximity error.
2. The acoustic centers are properly chosen.
3. The system and the medium are stable.
4. The receiving system is linear.
5. The transducers are properly rigged.
6. There is no boundary interference or electrical crosstalk.

The distance-loss test might fail at a single frequency because two errors of different kinds might cancel each other. However, if this test is made at several frequencies or over a wide enough frequency range, the probability of failure is very low.

Assuming that all of the conditions have been met, we can proceed with the calibration. The open-circuit output voltage e_s of the standard hydrophone is measured. Then the open-circuit output voltage e_x of the unknown is measured. If the free-field voltage sensitivity of the standard hydrophone is M_s, then the sensitivity of the unknown M_x

is found from

$$M_x = \frac{M_s e_x}{e_s}$$

or in decibels

$$20 \log M_x = 20 \log M_s + 20 \log e_x - 20 \log e_s.$$

Usually the sensitivity of the calibrated hydrophone will be expressed in decibels reference to 1 volt per micropascal and will range in value from approximately -170 dB to -210 dB. If the reference is a microbar it will change these values to -70 dB to -110 dB as noted earlier.

Figure 4 shows a typical free-field voltage sensitivity for a broadband hydrophone type H52. This hydrophone has a transistor preamplifier located near the lithium sulfate crystal sensor element. The output voltage was measured at the end of the 23-meter cable and includes the gain of the preamplifier. A typical strip chart recording of the output voltages of a standard hydrophone such as the H52 and an unknown hydrophone when placed in the sound field produced by a moving-coil type projector is shown in Fig. 5.

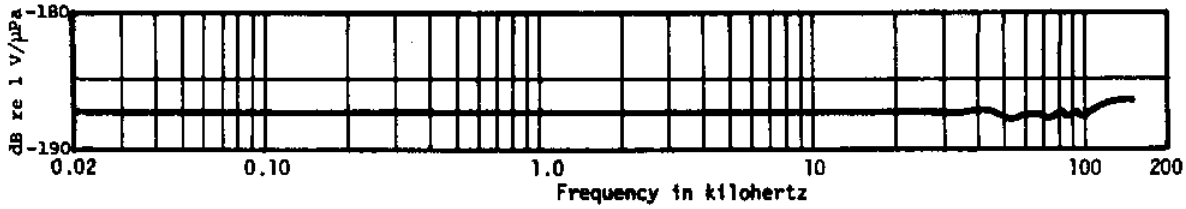

Fig. 4. Typical free-field voltage sensitivity, type H52 hydrophone; open-circuit voltage at end of 23-m cable.

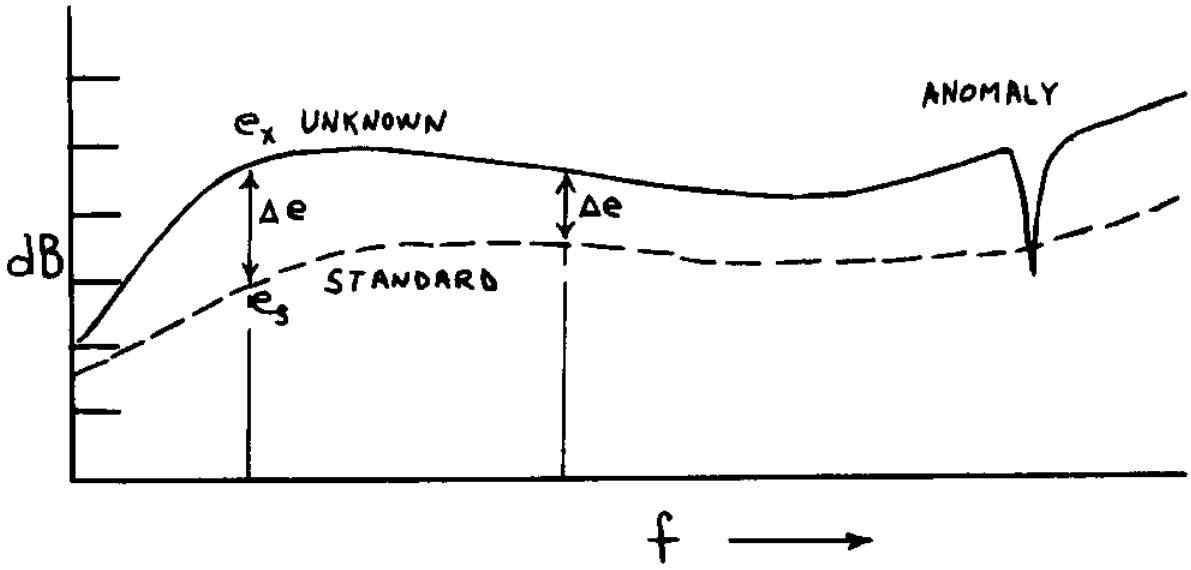

FIG. 5. Typical strip-chart recording of the output voltages of a standard H52 hydrophone and an unknown hydrophone.

In each case the plotted output voltage includes the characteristics of the projector. However, as long as the projector is stable and the sound pressure produced during the measurement of the two hydrophones is the same, we can easily determine the sensitivity of the unknown hydrophone by taking the difference between the two curves and either add or subtract, as the case may be, these values from the free-field voltage sensitivity curve of the standard.

We will look in more detail at some of these conditions which must be satisfied for calibration measurements. Number 6 is a problem frequently found in most measurements in practical situations. If we had a true free field there would be no boundary interference but electrical crosstalk could still exist. Some of the possible paths of interfering signals are shown in Fig. 6.

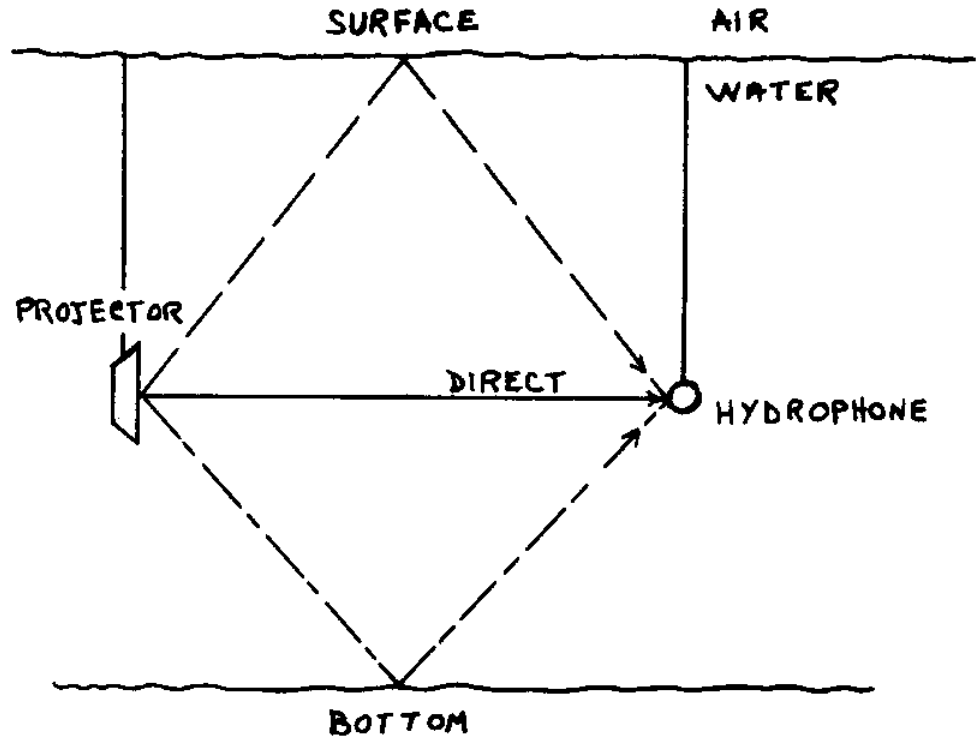

FIG. 6. Possible interference due to surface or bottom reflections.

The magnitude of the components arising from the interference depends upon the directivity of the transducers. When the data are recorded on a strip chart, as is usually the case at the NRL-USRD, the operator makes a subjective estimate of the average value of the oscillation caused by the interference. Fig. 7 shows an exaggerated plot of the measured hydrophone output voltage versus frequency for a typical oscillating interference pattern resulting from a surface reflection. The solid line is the measured sum of direct and reflected signals while the dashed line is the computed direct signal.

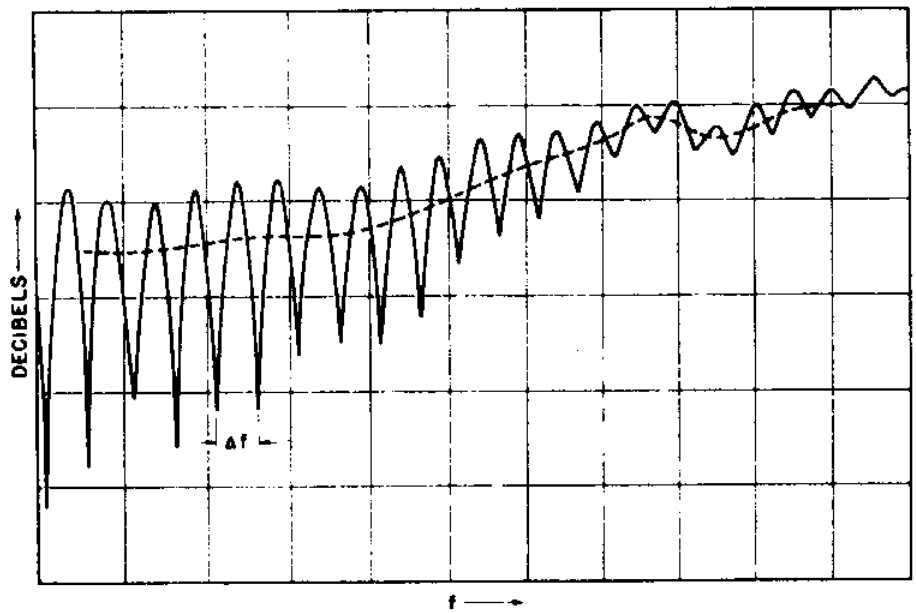

Fig. 7. Measured hydrophone output voltage versus frequency, illustrating a typical oscillating interference pattern resulting from a surface reflection. Solid line is measured sum of direct and reflected signals. Dashed line is computed direct signal.

The oscillating pattern can be identified as a surface reflection interference from

$$\Delta f = c/\Delta d$$

where Δf is the frequency interval between adjacent peaks or adjacent nulls, c is the speed of sound in the medium, and Δd is the path difference between the direct and the surface reflected signals.

Bobber[1] has made an analysis of the problem and has shown that when the transducers are half way between the water-air surface and a bubble pressure-release bottom is present, the true frequency response curve has superimposed upon it an interference pattern which is a sequence of saw-tooth and peak-wave shapes. For a projector-to-hydrophone distance equal to one-tenth to one-eighth of the total water depth, the interference wave shapes can be expected to have amplitudes of 7 to 8 dB. Fig. 8 shows the condition for transducers separated by a distance equal to 1/8 of the water depth.

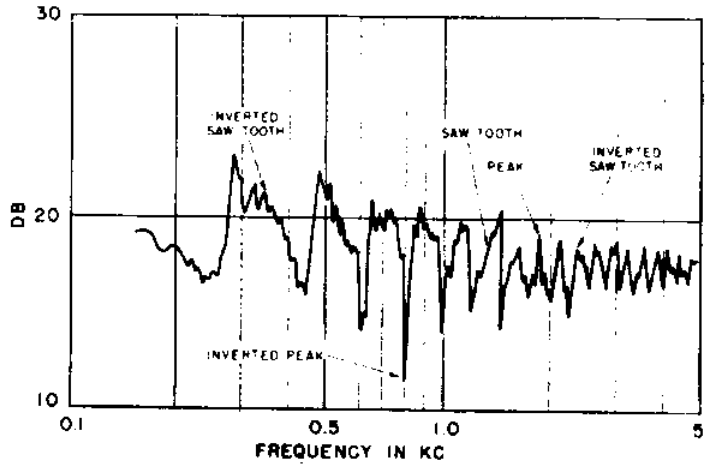

Fig. 8. Measured hydrophone output voltage where projector and hydrophone both are at a depth midway between the water-air surface and bubble-covered bottom. The transducers are separated by a distance equal to 1/8 of the water depth. The projector transmitting response and hydrophone receiving sensitivity both are essentially constant with frequency.

It is quite apparent that a single measurement of the sound field at a single frequency could produce considerable error under the above conditions. Conditions can be improved by using pulse measurements rather than c-w. Likewise the measurement can be quite good if in a calibration process the comparison method is used and the standard and the unknown transducer have essentially the same directivity characteristics. Both would be subject to the same variations and the measured output voltage of each hydrophone should be proportional.

Conventional Reciprocity[2]

A conventional reciprocity calibration requires three transducers of which one serves as a projector P, one is a reciprocal transducer T and serves as both a projector and hydrophone, and one serves only as a hydrophone H. Anyone of the three transducers can be the unknown or the one being calibrated; however, the calibration formula usually is derived for the free-field voltage sensitivity M_H of the hydrophone. The measurements are made in free field under free-field conditions so that only spherical waves from the projector impinge on the hydrophone.

The arrangements and measurements required are shown schematically in Fig. 9 a, b, and c.

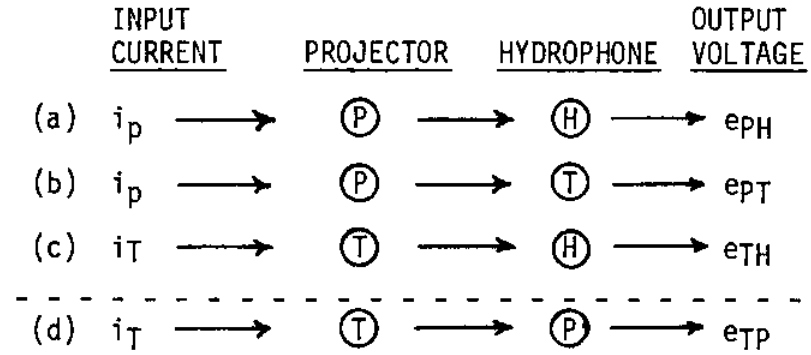

FIG. 9. Diagram of the three measurements (a), (b), & (c) for a reciprocity calibration

One additional measurement can be made for a reciprocity check on the reversible transducer T as shown in (d).

The free-field voltage sensitivity M_H of the hydrophone is obtained from the first three measurements as follows. The free-field sound pressure p_P produced by P at the position of H or T, d_1 centimeters from P, is $i_p\ S_p\ d_o/d_1$, where S_p is the transmitting current response of P and d_o is the reference distance in centimeters at which the transmitted pressure is specified in the definition of S_p (usually 100 cm). Then,

$$e_{PH} = M_H\ P_P = \frac{M_H\ i_p\ S_p\ d_o}{d_1} \tag{1}$$

and

$$e_{PT} = M_T\ P_p = \frac{M_T\ i_p\ S_p\ d_o}{d_1} \tag{2}$$

where M_T is the free-field voltage sensitivity of T. From Eqs. (1) and (2)

$$\frac{e_{PH}}{e_{PT}} = \frac{M_H}{M_T} \tag{3}$$

If T is a reciprocal transducer,

$$\frac{M_T}{S_T} = J \tag{4}$$

and from equations (3) and (4),

$$M_H = \frac{J\ S_T\ e_{PH}}{e_{PT}} \tag{5}$$

The free-field sound pressure p_T produced by T at the position H, d_1 centimeters from T, is $i_T\ S_T\ d_0/d_1$, where S_T is the transmitting current response of T. Then,

$$e_{TH} = M_H\ p_T = \frac{M_H\ i_T\ S_T\ d_0}{d_1} \tag{6}$$

and from equations (5) and (6),

$$M_H = \left[\frac{e_{TH}\ e_{PH}}{e_{PT}\ i_T}\ \frac{d_1}{d_0}\quad J\right]^{1/2}. \tag{7}$$

The reciprocity parameter J is derived in the literature and is equal to $(2d_0/\rho f)10^{-7}$, where ρ is the density of the medium in grams per cubic centimeter and f is the frequency in Hertz. The factor 10^{-7} appears from the use of a mixed system of units, since the dimension of J is volt-amperes/microbar. The voltage and current are measured in MKS volts and amperes. The distance, density, and pressure are measured in CGS units. The ratio d_1/d_0 does not usually appear in equation (7) because either the voltages are corrected to what they would be if d_1 = 100 cm and $d_1/d_0 = 1$, or $(d_1/d_0)(2d_0/\rho f)$ is combined. That is J is defined as $2d_1/\rho f$ instead of $2d_0/\rho f$. When voltage corrections are used, it must be remembered that the voltage is proportional to the sound pressure, not the intensity. In a spherically divergent wave, the voltage therefore is proportional to the distance, not the distance squared. Assuming that $d_1 = d_0$ or that $J = 2d_1/\rho f$, equation (7) becomes

$$M_H = \left[\frac{e_{PH}\ e_{TH}}{e_{PT}\ i_T}\ J\right]^{1/2} \tag{8}$$

If H is now used as a calibrated hydrophone standard, P and T can be calibrated by secondary calibration methods, such as the comparison method. If the projector P is also a reciprocal transducer and the additional measurement (d) in Fig. 9 is made, then measurements (b) and (d) constitute the reciprocity check; that is, both P and T are assumed reciprocal if $e_{PT}/i_P = e_{TP}/i_T$. From measurements (a), (c), and (d),

$$M_H = \left[\frac{e_{TH}\, e_{PH}}{e_{TP}\, i_P}\, J\right]^{1/2} \tag{9}$$

The numerators of equations (8) and (9) are identical and the denominators are equal. The addition of a fourth measurement to the necessary three provides both a reciprocity check and some redundancy that increases the reliability of the measurements.

It can be seen from equation (8) that the electrical standard in a reciprocity calibration is an e/i ratio or an impedance. The current i_T can be measured as the voltage drop e_T across a standard impedance--usually a resistance R. Then equation (8) becomes

$$M_H = \left[\frac{e_{PH}\, e_{TH}\, R}{e_{PT}\, e_T}\, J\right]^{1/2} \tag{10}$$

Standard Hydrophones

Measurement transducers usually consist of standard hydrophones and sound sources or projectors. The primary requirements of a standard are stability and linearity. The sensitivity of a standard hydrophone should be independent of time, frequency, temperature, and hydrostatic pressure. If the sensitivity does change as a function of any of these parameters, it should change in a predictable and repeatable manner.

Standard hydrophones are usually designed for a frequency bandwidth of two or more decades. The sensor element is normally made small to provide as omnidirectional characteristics as possible. In practical cases for standard hydrophones, the sensor is designed to provide an omnidirectional response in one plane (usually the XY plane, normal to the length axis of the hydrophone). The XZ plane (vertical) will normally have some directivity due to the finite length of the sensor which may be from 1-cm to 5-cm long. In some measurements, vertical directivity is desired and a standard will consist of six or more small capped piezoelectric tubes mounted one above the other to form a line hydrophone 15 cm or more in length. Typical standard transducers illustrating both types are the USRD type H52 hydrophone and the type F37 transducer. The type H52 dimension and the directivity patterns for the XY and XZ planes are shown in Figs. 10, 11, and 12. The dimensions of the type F37, the free-field voltage sensitivity, transmitting voltage response, and the directivity patterns in the XZ plane (vertical) are shown in Figures 13, 14, 15, and 16. The type F37 is omnidirectional in the XY plane $\pm$0.5 dB to frequencies as high as 37 kHz.

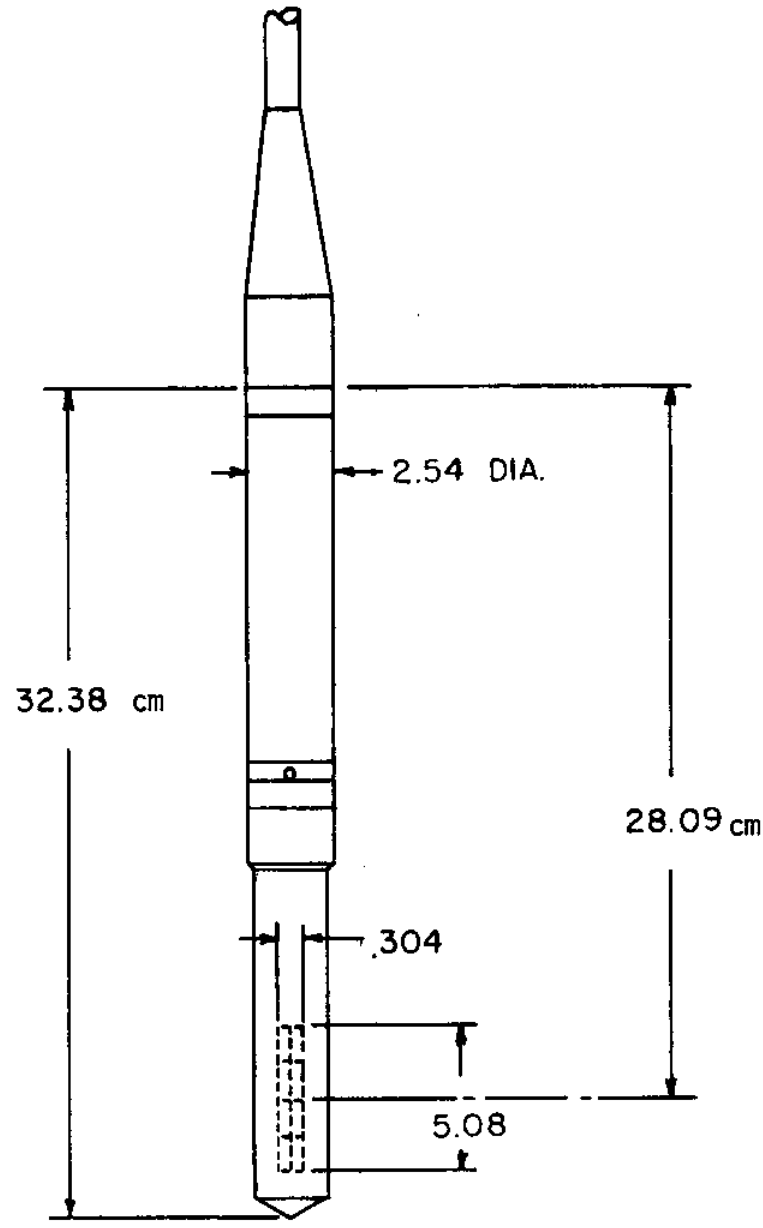

FIG. 10. Dimensions of type H52 standard hydrophone.

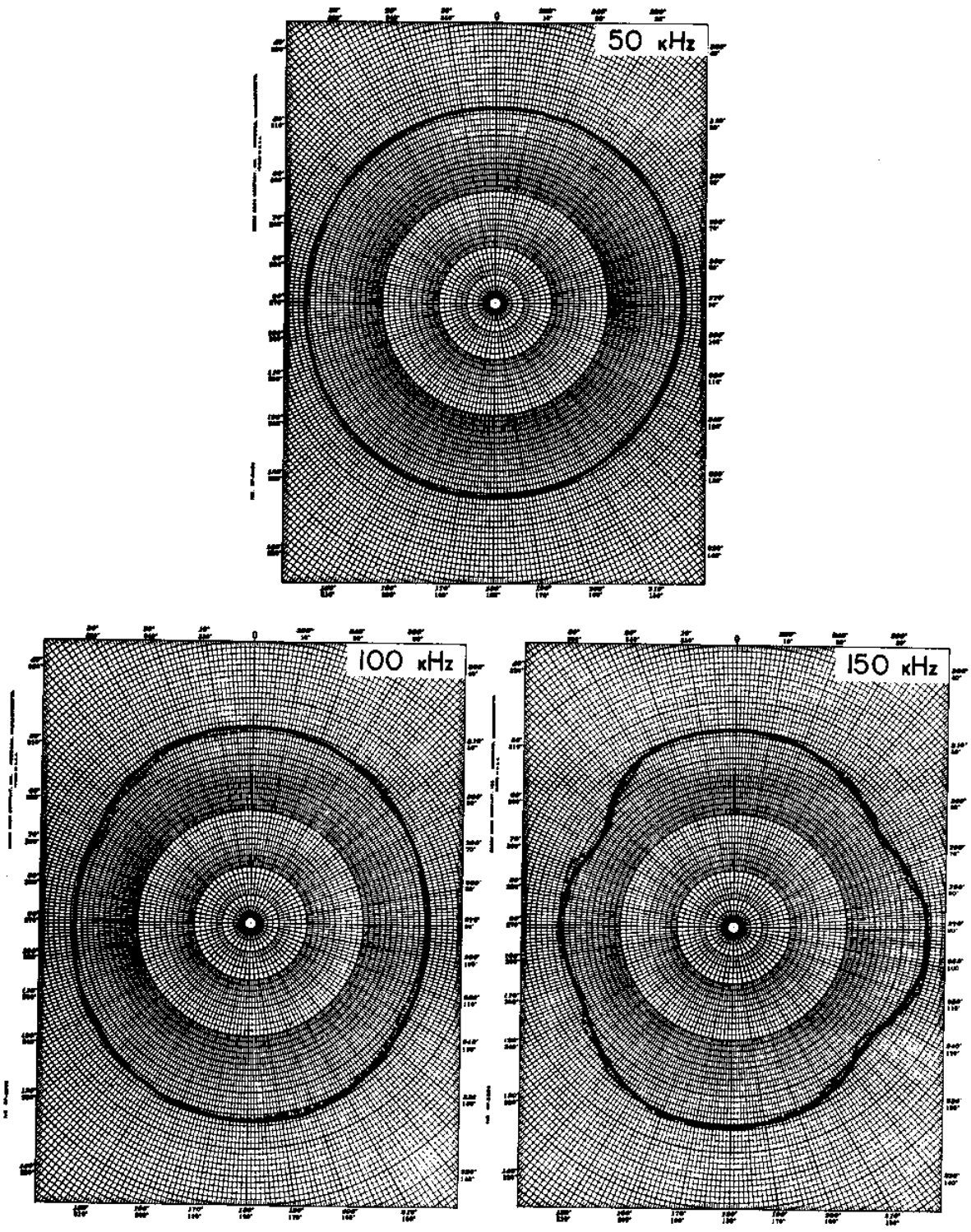

Scale: Center to top of grid, each pattern, equals 50 dB.

Fig. 11. Typical directivity patterns in the XY plane, USRD type H52 hydrophone; dashed lines indicate effect of protective wire guard around the hydrophone.

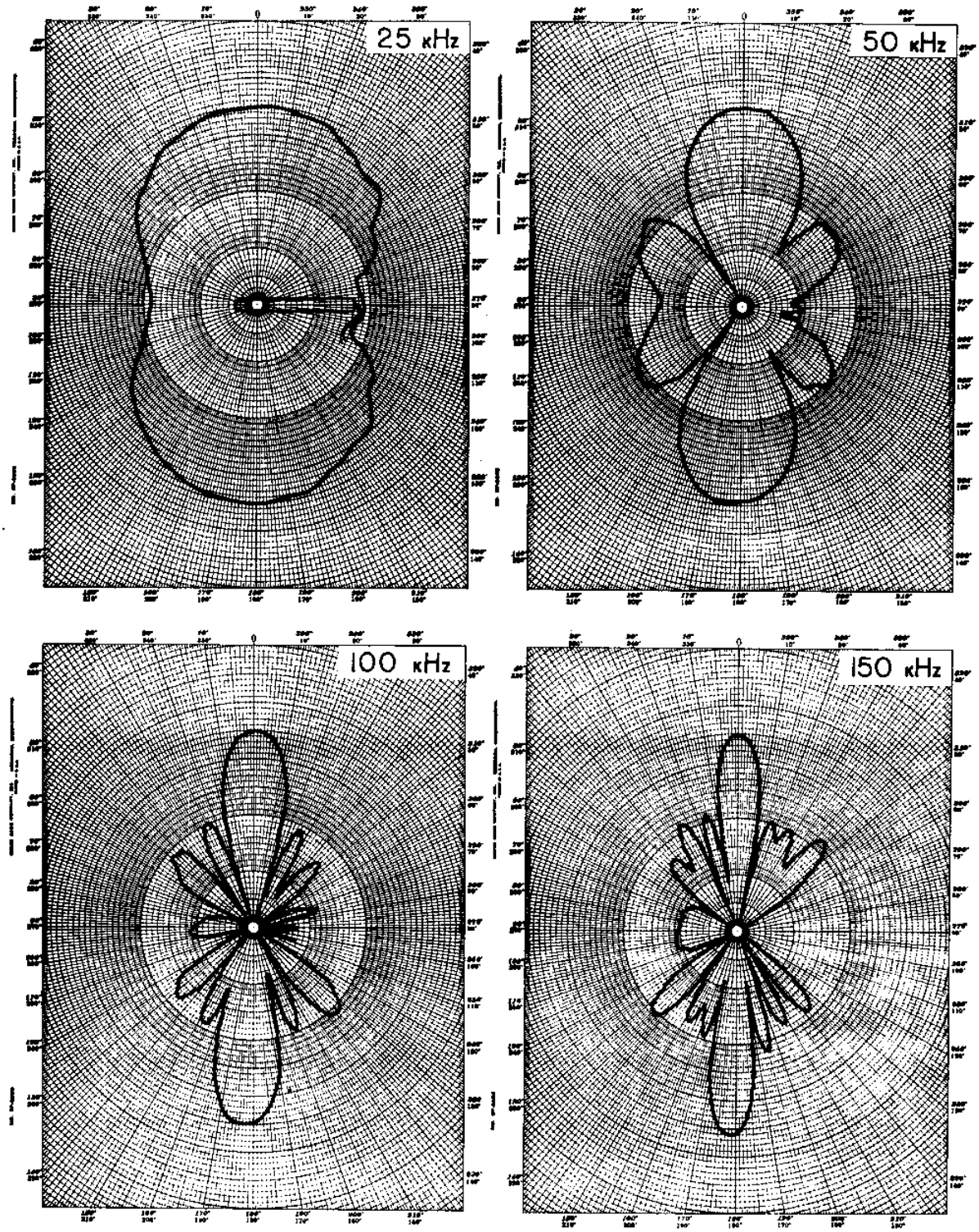

Scale: Center to top of grid, each pattern, equals 50 dB.

Fig. 12. Typical directivity patterns in the XZ plane, USRD type H52 hydrophone.

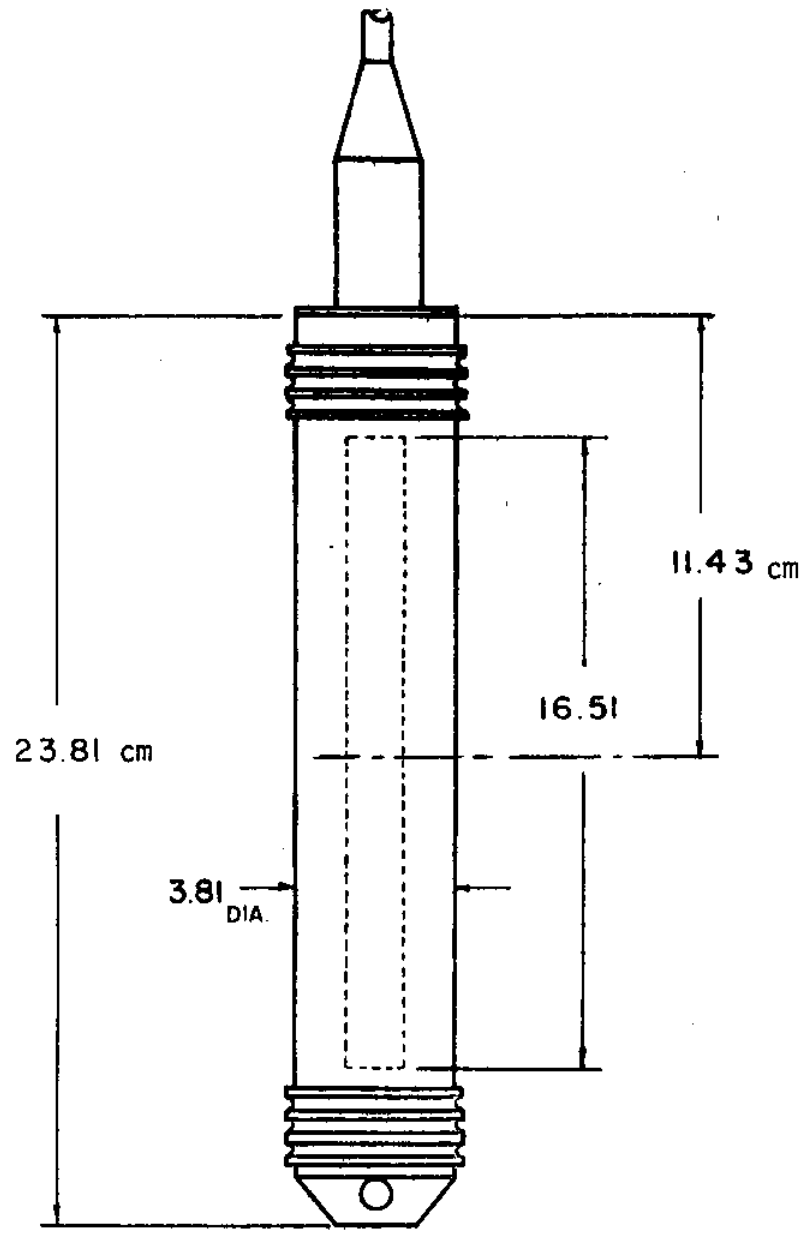

FIG. 13. Dimensions of type F37 standard transducer.

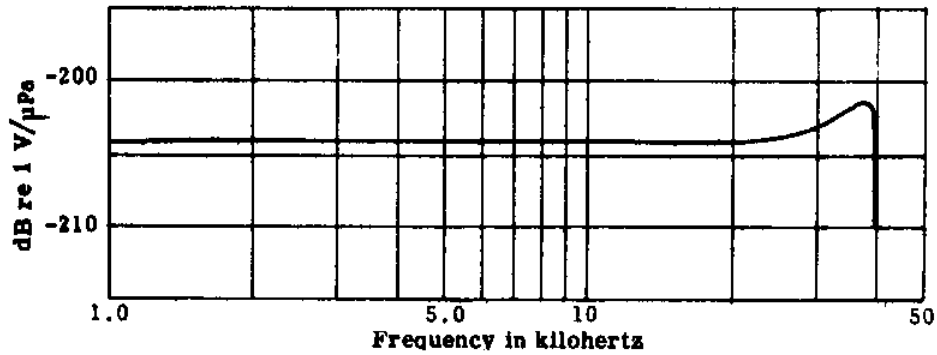

Fig. 14. Typical free-field voltage sensitivity, USRD type F37 transducer (open-circuit voltage at end of 30.5-m cable); unbalanced: shield and black lead grounded.

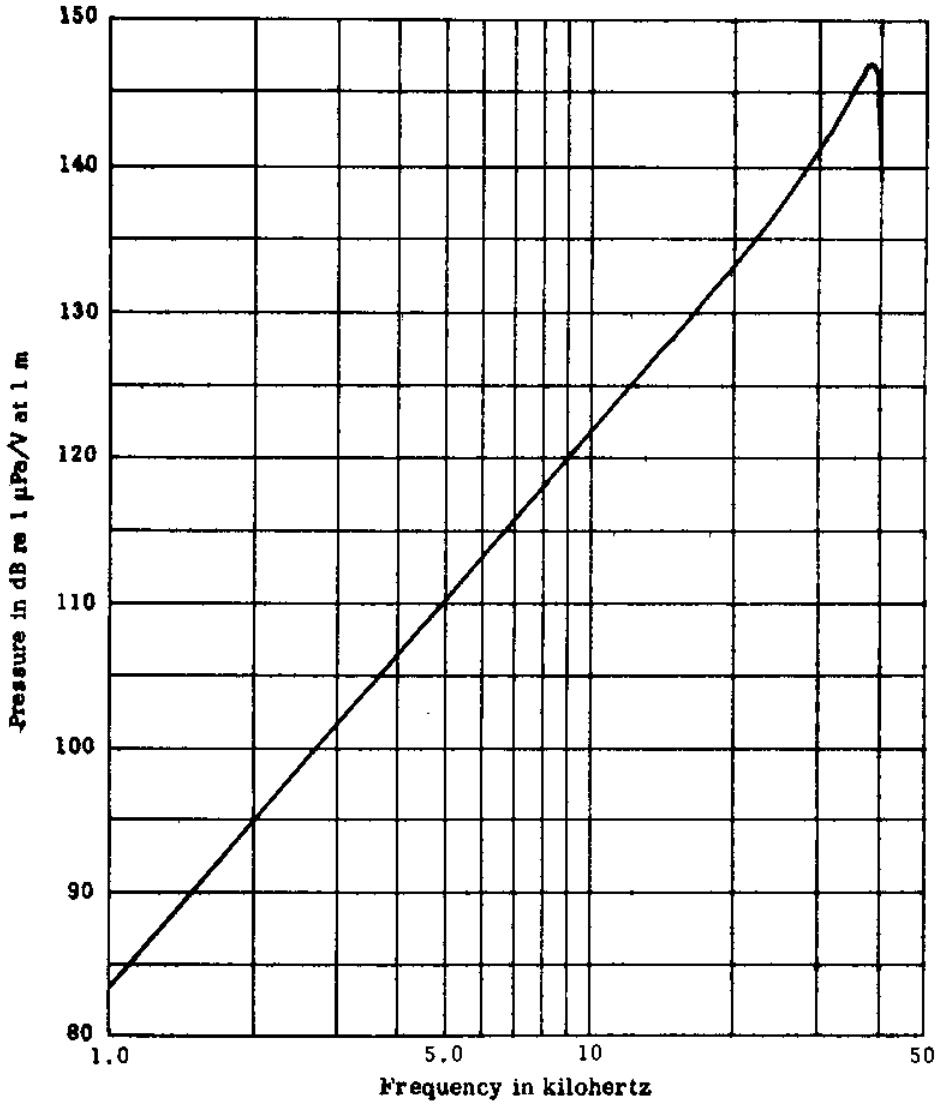

Fig. 15. Typical transmitting voltage response, USRD type F37 transducer; unbalanced: shield and black lead grounded.

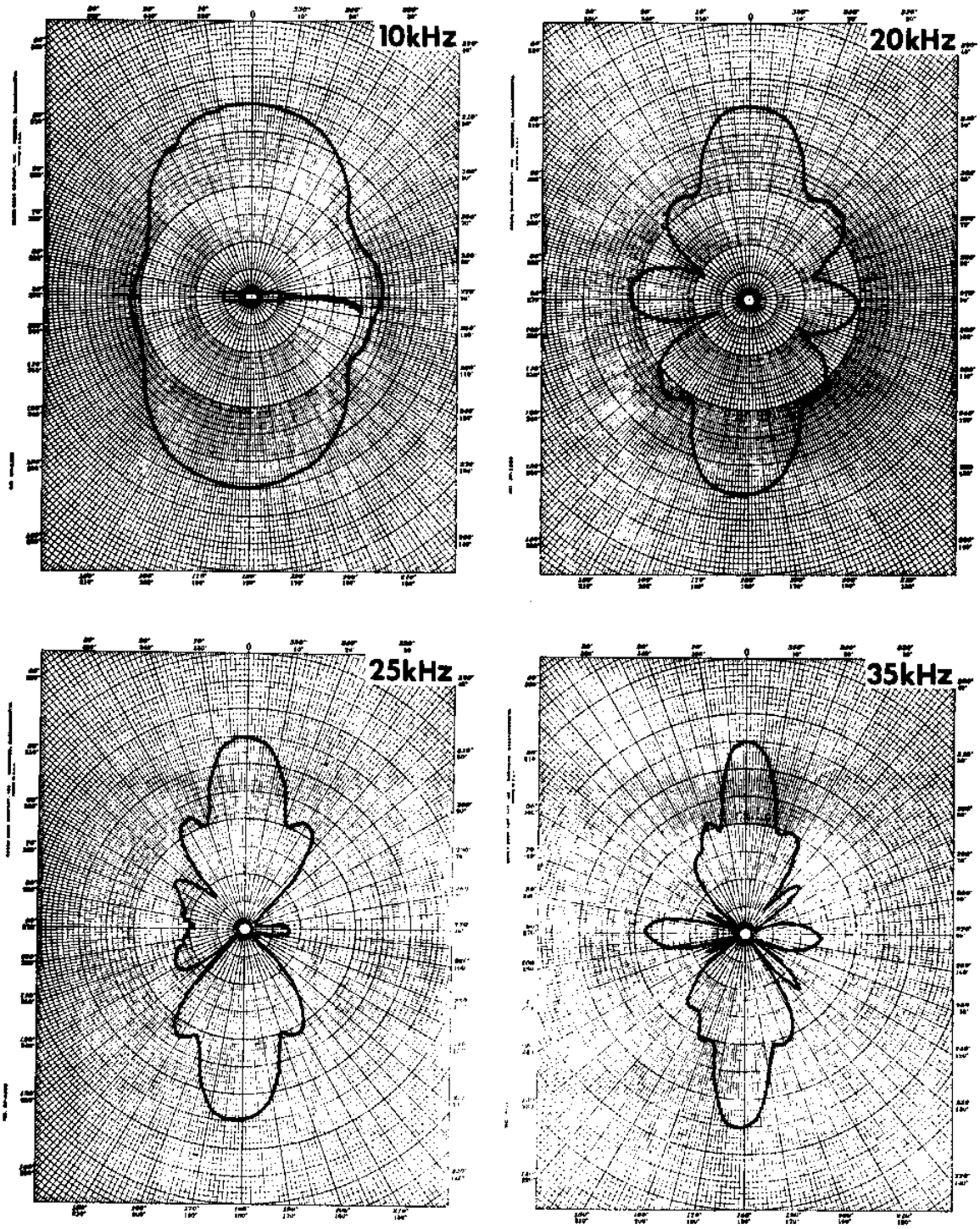

Scale: Center to top of grid, each pattern, equals 50 dB

Fig. 16. Typical directivity patterns in the XZ plane, USRD type F37 transducer.

Some measurements require a standard hydrophone with adequate sensitivity and low self-noise to provide an equivalent sound pressure less than that of Sea State Zero. This requirement is not too difficult to meet if the measurements are to be made below 10 kHz. Sensor elements sensitivity, impedance, frequency range, and directivity characteristics are determined largely by the size of the element. If the sensor element is large enough, high sensitivity and low impedance can be obtained with a low equivalent noise pressure. However, the large element will have resonances at lower frequencies and diffraction will occur at lower frequencies due to the finite size and these tend to limit the frequency range over which the response characteristics are smooth and free of anomalous behavior. As the size of the sensor element is reduced in order to make it small compared to the wavelength and thus maintain its omnidirectional characteristics, the sensitivity decreases and usually the impedance must also increase. Thus the design of the hydrophone becomes a trade-off of sensitivity and low impedance on one hand and frequency bandwidth and omnidirectionality on the other. Figures 17 and 18 show the equivalent noise pressure and illustrate the design trade-offs as found in the type H52 and type H56 hydrophones. The H52 uses a lithium sulfate crystal with a capacitance of approximately 32 pF and an open-circuit crystal sensitivity of -193.6 dB re 1 volt per micropascal. The H52 can be used to frequencies higher than 150 kHz. The H56 has a piezoelectric ceramic sensor element using an area ratio type design with a capacitance of 100 pF and an open-circuit crystal sensitivity of -183 dB re 1 volt per micropascal. The equivalent noise pressure of the H56 is lower than the H52 but at a sacrifice of bandwidth. The free-field voltage sensitivity curve for the H56 is shown in Fig. 19, and it can be seen that the usefulness is limited above 70 kHz.

Another important factor traded off for the lower equivalent noise pressure is that of stability with hydrostatic pressure. The lithium sulfate sensor in the H52 can be used to very high pressures in excess of 70 MPa ($\approx$10,000 psi) or 7000 meters depth with little change in sensitivity. Due to the design of the H56 sensor the pressure must be limited to approximately 7 MPa ($\approx$ 1000 psi) to avoid excessive sensitivity changes or complete failure at even higher pressures.

Hydrostatic Pressure Stability[3]

Many hydrophones have been designed and used at great ocean depths where little has been known about the sensitivity characteristics as a function of hydrostatic pressure. It is not unusual to have sensitivity changes of more than 6 dB with hydrostatic pressures of less than 7 MPa (1000 psi). It is important that the designer take this into consideration if the measurements are to be made where the pressure exceeds more than 690 kPa (100 psi) as some designs can even change sensitivity at lower pressures. Fig. 20 shows some of the ceramic element configurations which might be used. Capped tubes and hollow spheres are limited

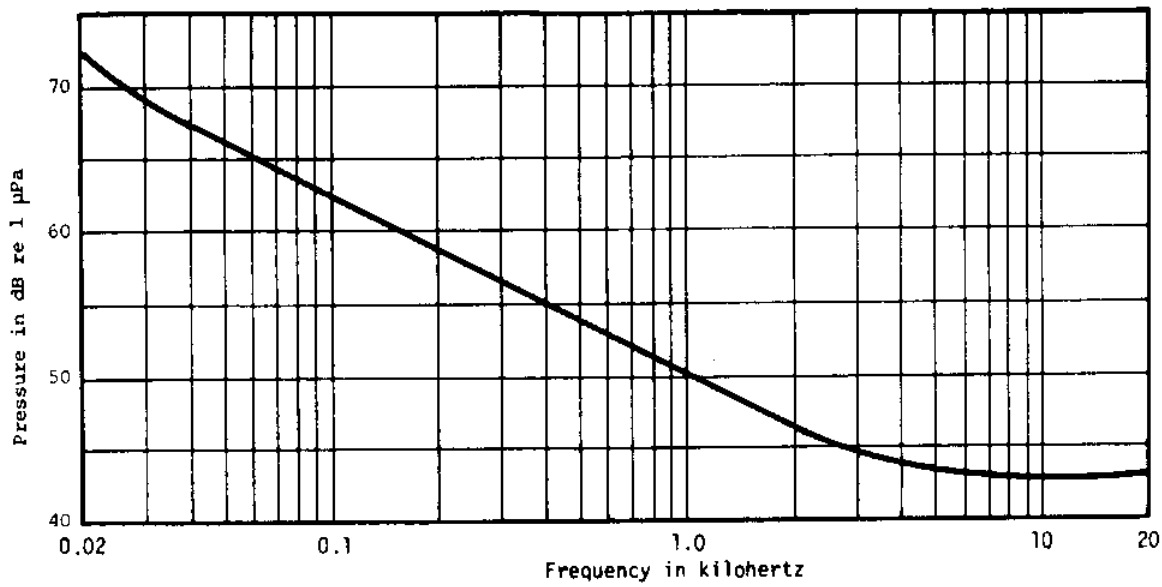

FIG. 17. Typical equivalent noise pressure, USRD Type H52 hydrophone.

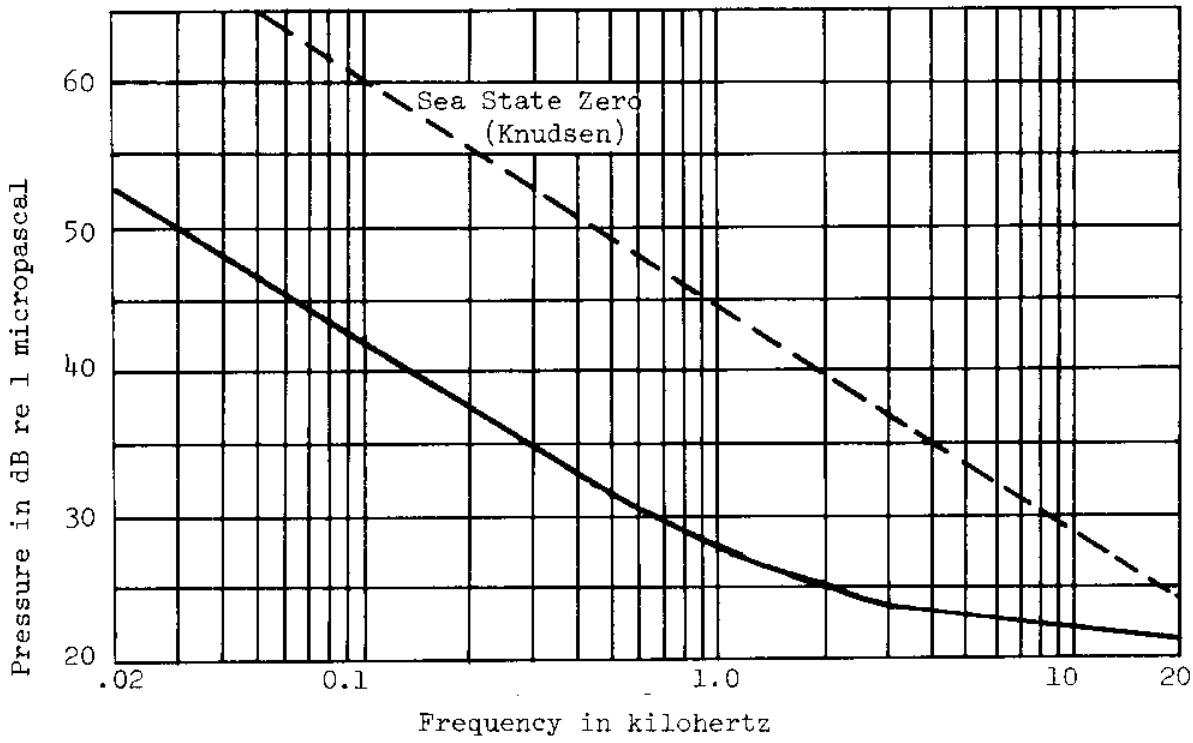

FIG. 18. Typical equivalent noise pressure, USRD Type H56 Hydrophone.

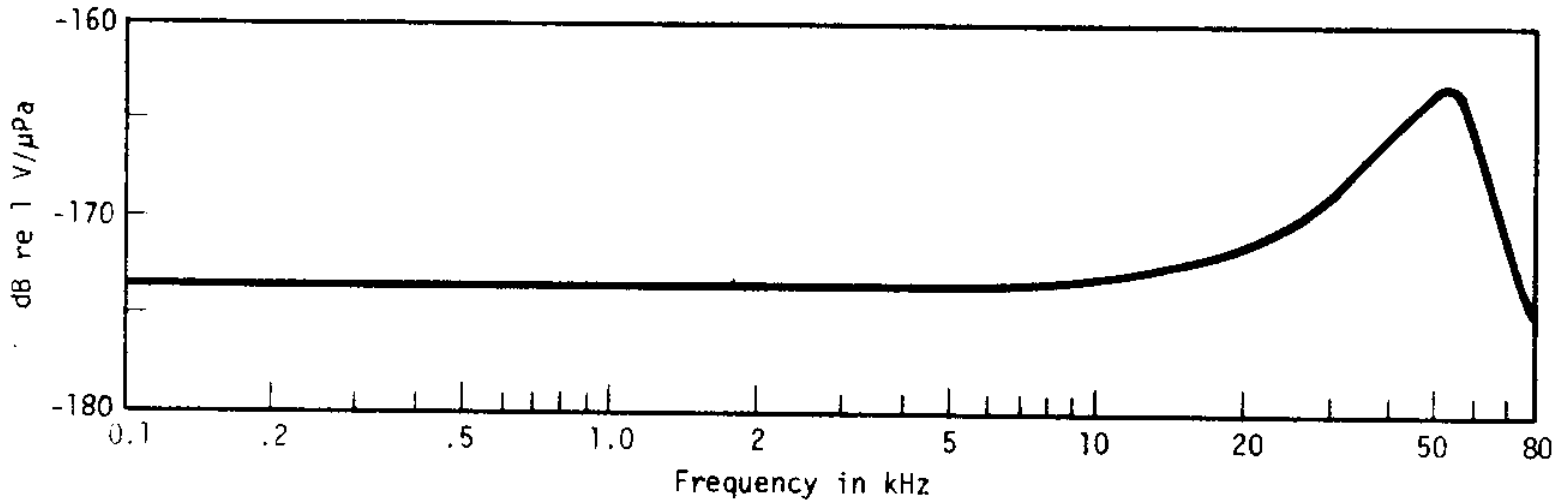

FIG. 19. Typical free-field voltage sensitivity, USRD Type H56 hydrophone.

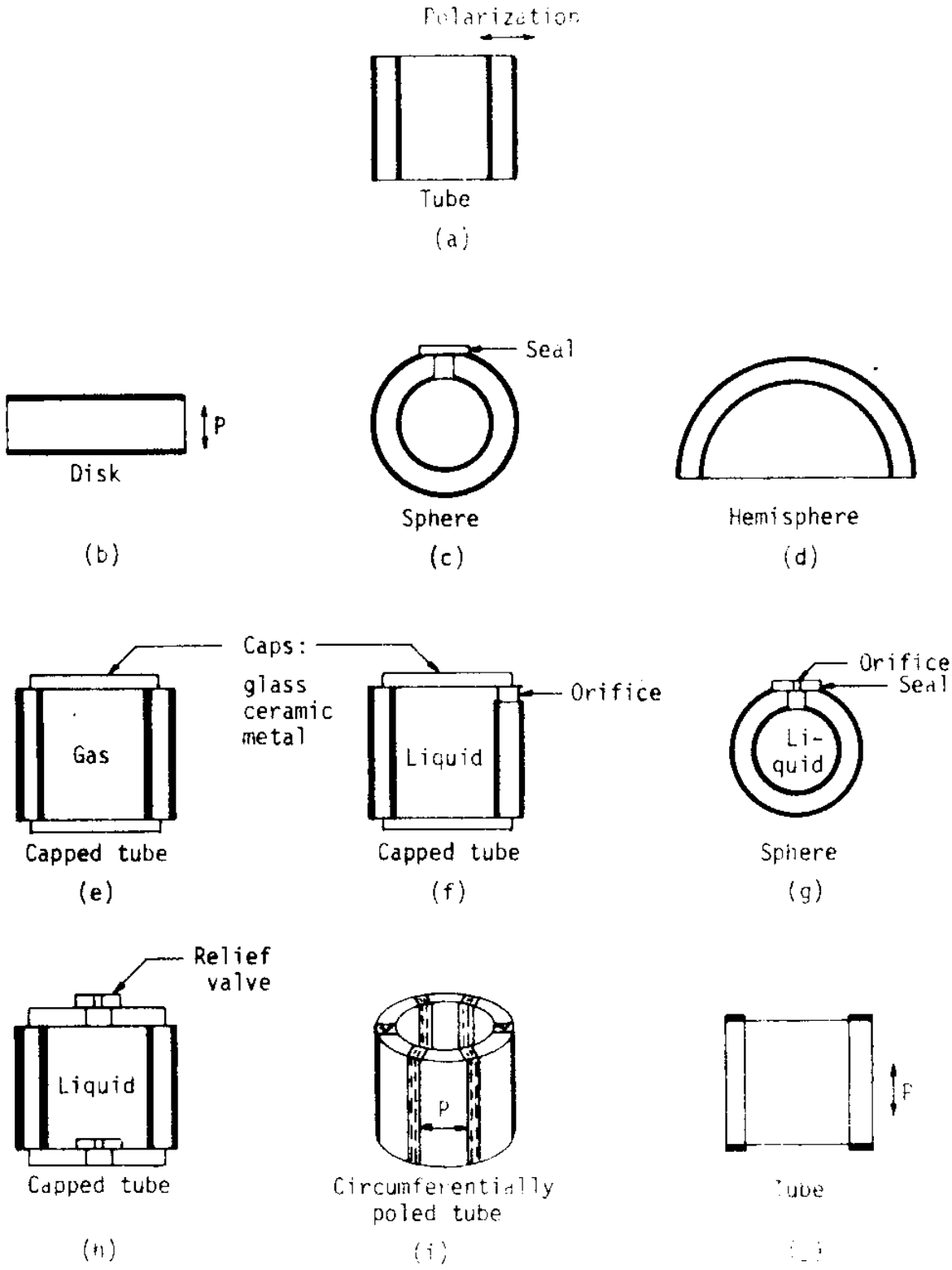

FIG. 20. Configurations of piezoelectric ceramic sensor elements.

in the maximum pressure they can withstand without mechanical failure or change in their electroacoustic characteristics. As the radius of the tube or sphere is increased and as the wall thickness is decreased, the maximum hydrostatic pressure must also be decreased. If higher pressures are required than can be tolerated by the air-filled elements, then some pressure-compensation method must be used. Both the capped tube and the hollow sphere can be used if a small orifice is provided to permit the oil to fill the inside of the tube and sphere as shown in Fig. 20 (f) and (g). The small orifice serves as a low-pass acoustic filter or offers high acoustic impedance but permits the hydrostatic pressure to equalize with the pressure at the operating depth. The sensitivity of the tube or sphere will decrease 3 dB or more when used in this manner, but the sensitivity will then be stable with hydrostatic pressures to very high values.

Lithium sulfate is outstanding in its stability with both temperature and pressure variations. Since it is a volume expander, this crystal is used in most applications without an acoustic pressure-release material on any surface. This fact alone improves its stability as a function of hydrostatic pressure. The piezoelectric hydrostatic moduli is high and is only about 20% less than the g_{33} piezoelectric moduli. Lithium sulfate may be used to pressures in excess of 100 MPa ($\approx$15,000 psi) with less than 0.3-dB change in sensitivity.

One other material worth noting is lead metaniobate, $Pb(NbO_3)_2$, a ferroelectric ceramic that is also a volume expander. It is not quite as stable as lithium sulfate, but it may be used to high hydrostatic pressures with little change in sensitivity. Unlike lithium sulfate it is a ceramic and is not water soluble--a decided advantage when used in underwater transducers.

Practical Equations for Calculating Sensitivity of Various Piezoelectric Ceramic Sensor Configurations

Capped Tube

The free-field voltage sensitivity for the capped piezoelectric ceramic tube can be computed from the equation

$$\frac{V}{p_o} = b\left(g_{33}\frac{1-\rho}{1+\rho} + g_{31}\frac{2+\rho}{1+\rho}\right), \qquad (1)$$

where V is the open-circuit output voltage developed by the element, a and b in meters are the inner and the outer radii, respectively, of the ceramic tube; g_{33} and g_{31} are the electromechanical voltage constants of the ceramic material; $\rho = a/b$ is the ratio of the inner to the radius; and p_o is the external pressure in newtons per square meter (pascals).

Nominal values for the electromechanical voltage constants of PZT-4 are $g_{33} = 24.9 \times 10^{-3}$ V·m/N and $g_{31} = -10.6 \times 10^{-3}$ V·m/N. Let the dimensions of the element be: outer radius b = 9.52×10^{-3} m (0.375 in.), and inner radius a = 7.95×10^{-3} m (0.313 in.). So, $\rho = 0.835$.

Then, substituting p_o = 1 dyne/cm^2 (1 microbar, or 10^{-1} Pa) in Eq. (1) yields

$$V = 13.2 \times 10^{-6} \text{ V/microbar.}$$

If p_o = 1 micropascal (10^{-6} N/m^2), then

$$V = 13.2 \times 10^{-11} \text{ V/micropascal,}$$

which is the free-field voltage sensitivity M_o of the element when the dimensions are small in comparison with the wavelength. Expressed in decibels,

$$M_o = 20 \log 13.2 \times 10^{-6} = -97.6 \text{ dB re 1 V/microbar, or}$$

$$M_o = 20 \log 13.2 \times 10^{-11} = -197.6 \text{ dB re 1 V/micropascal.}$$

Disk or Plate

For the sensitivity of a disk or plate, when the sound pressure is impinging on the major surfaces and the size of the element is small in comparison with a wavelength,

$$V/p_o = g_{33}t, \tag{2}$$

where g_{33} is the electromechanical voltage constant of the piezoelectric material, t is the thickness in meters, and p_o is the pressure in newtons per square meter (pascals).

A nominal value for the electromechanical voltage constant for lithium sulfate as a thickness expander is $g_{33} = 175 \times 10^{-3}$ V·m/N. When the plate is used as a volume expander, the value $g_{33} = 148 \times 10^{-3}$ V·m/N should be used.

Let the thickness t = 1.524×10^{-3} m (0.060 in.). Then substituting p_o = 1 dyne/cm^2 (10^{-3} Pa) in Eq. (2) yields

$$V = 26.67 \times 10^{-6} \text{ V/microbar} = 26.67 \times 10^{-11} \text{ V/micropascal,}$$

which is the free-field voltage sensitivity M_o of the element. Expressed in decibels,

$$M_o = 20 \log 26.67 \times 10^{-6} = -91.48 \text{ dB re 1 V/microbar, or}$$

$$M_o = 20 \log 26.67 \times 10^{-11} = -191.48 \text{ dB re 1 V/micropascal.}$$

Hollow Sphere

The free-field voltage sensitivity of a piezoelectric ceramic hollow sphere can be computed from the relation

$$\frac{V}{p_o} = \frac{b}{(\rho^2 + \rho - 1)} \left[g_{33} \frac{(\rho^2 + \rho - 2)}{2} - g_{31} \frac{(\rho^2 + \rho - 4)}{2} \right], \qquad (3)$$

where $\rho = a/b$ and a and b in meters are the inner and outer radii, respectively, of the sphere.

For a thin-walled sphere where $a \to b$, a close approximation to the free-field voltage sensitivity is given by

$$V/p_o = -bg_{31}. \qquad (4)$$

Let the dimensions be: $a = 2.22 \times 10^{-2}$ m (0.875 in.) and $b = 2.54 \times 10^{-2}$m (1.0 in.); $a/b = 0.875$. For PZT-5, $g_{33} = 24.8 \times 10^{-3}$ V·m/N and $g_{31} = -11.4 \times 10^{-3}$ V·m/N. Substituting the appropriate values in Eq. (3) yields

$$V/p_o = 26.647 \times 10^{-5} \text{ V/Pa}.$$

If the reference pressure is 1 micropascal = 10^{-6} Pa, then

$$M_o = 20 \log 26.647 \times 10^{-11} = -191.5 \text{ dB re 1 V/micropascal}.$$

The value obtained by using the approximation, Eq. (4), is $V/p_o = (-2.54 \times 10^{-2})(-11.4 \times 10^{-3}) = 28.95 \times 10^{-5}$ V/Pa, or

$$M_o = 20 \log 28.95 \times 10^{-11} = -190.8 \text{ dB re 1 V/micropascal}.$$

which is in close agreement with the value -191.5 dB obtained by using Eq. (3).

Projectors

Two types of projectors are normally used in calibration measurements. The moving-coil (dynamic) type is used in the audio and subaudio frequency range 10 Hz to 20 kHz. Piezoelectric measurement projectors are designed for operation below resonance in the stiffness-controlled frequency range of the piezoelectric elements and are usually not used lower than 1 kHz. Below this frequency, the amount of ceramic or crystal becomes too great to be practical or economical and the driving voltage becomes excessive and may cause electrical breakdown. The NRL-USRD has standard crystal transducers which operate to frequencies as high as 2 MHz.

At low frequencies where the dimensions of the projector are small in comparison to a wavelength in water and the simple source concept is applicable, the transmitting voltage response curve has the slope 12 dB per octave as illustrated by the F37 transducer. This is due to the constant displacement per volt of the stiffness-controlled piezoelectric element. The transmitting current response curve has a 6-dB per octave slope.

The acoustic pressure produced at a radial distance r from a simple source is

$$|p| = \frac{\omega \rho U}{4\pi r} \tag{1}$$

where U is the rms volume velocity, p is the rms sound pressure, and ω is the angular frequency; also $U = \omega \xi A$, where ξ is the linear displacement of the radiating face or diaphragm and A is the radiating area.

From the definition of the piezoelectric moduli, d, (strain developed/applied field), $\xi = de$, where e is the applied voltage. Thus,

$$U = \omega \xi A = \omega de A. \tag{2}$$

Then the magnitude of the pressure per volt is

$$\frac{p}{e} = \frac{\omega^2 \rho d A}{4\pi r} \qquad \propto \omega^2 \tag{3}$$

The transmitting current response has the slope 6-dB per octave in the low-frequency region because the impedance is almost entirely a capacitive reactance; that is

$$\frac{p}{e} = \frac{p}{\frac{1}{j\omega C}} \tag{4}$$

where c is the electrical capacitance of the free element and i is the current. Then from Eqs. (3) and (4) above

$$\frac{p}{i} = \frac{\rho \omega^2 d A}{4\pi r} \frac{1}{\omega C} \qquad \propto \omega \tag{5}$$

At higher frequencies, where the transducer is not small in comparison to a wavelength, the simple source concept does not apply. The transmitting response then becomes dependent on the radiation impedance and directivity index.

Since $|p|$ is directly proportional to the volume velocity, U, it can be seen from Eqs. (1) and (2) that

$$|p| = \frac{\omega^2 \rho \xi A}{4\pi r} = \frac{\pi f^2 \rho \xi A}{r} \qquad (6)$$

where f is the frequency.

If the pressure is to remain constant as the frequency decreases, either the displacement or the area of the radiating face must become larger. Since the displacement of ferroelectric ceramics and piezoelectric crystals is very small, the moving-coil (dynamic) type transducer is usually used in the audio and sub-audio frequency ranges for projectors in calibration measurements.

Table 1 shows the displacement and piston area required to radiate 1 acoustic watt at specified frequencies from 10 Hz to 100 Hz.

TABLE 1

Frequency Hertz	Piston Area cm^2	Displacement cm
10	100	10.98
15	100	4.88
20	100	2.75
25	100	1.76
30	100	1.22
40	100	.69
50	100	.44
100	100	.109

The NRL-USRD has developed several moving-coil type transducers to meet most calibration requirements from 10 Hz to 20 kHz. The transmitting responses for the type J9 transducer are shown in Fig. 21 and

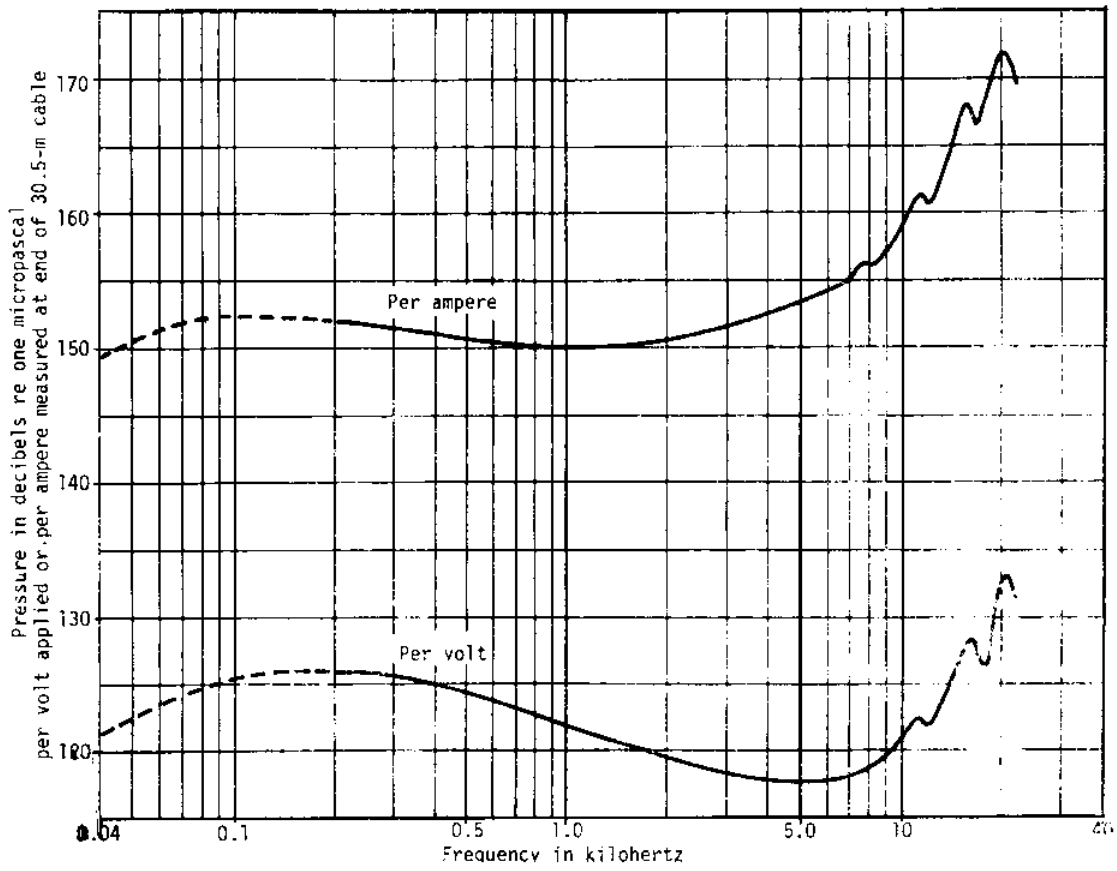

Fig. 21. Typical transmitting responses at 1 m, USRD type J9 transducer; response below 0.2 kHz is a function of depth.

the dimensions are provided in Fig. 22. When greater output and lower frequencies are required, the type J15-3, which uses three type J13 driver assemblies, is used. This transducer has a gas closed compensation system and may be used to depths of 200 meters. A typical transmitting current response for the J15-3 is shown in Fig. 23. The transducer may be driven with currents up to 3 amperes in the frequency range 50 to 500 Hz. The input current must be reduced at frequencies below 50 Hz due to the displacement limitation of the diaphragm. At frequencies above 500 Hz the input power must be reduced because of the heat generated in the driving coils. Since the impedance increases with increasing frequency, the I^2R loss becomes greater even when the current is kept constant. A typical impedance of the J15-3 is shown

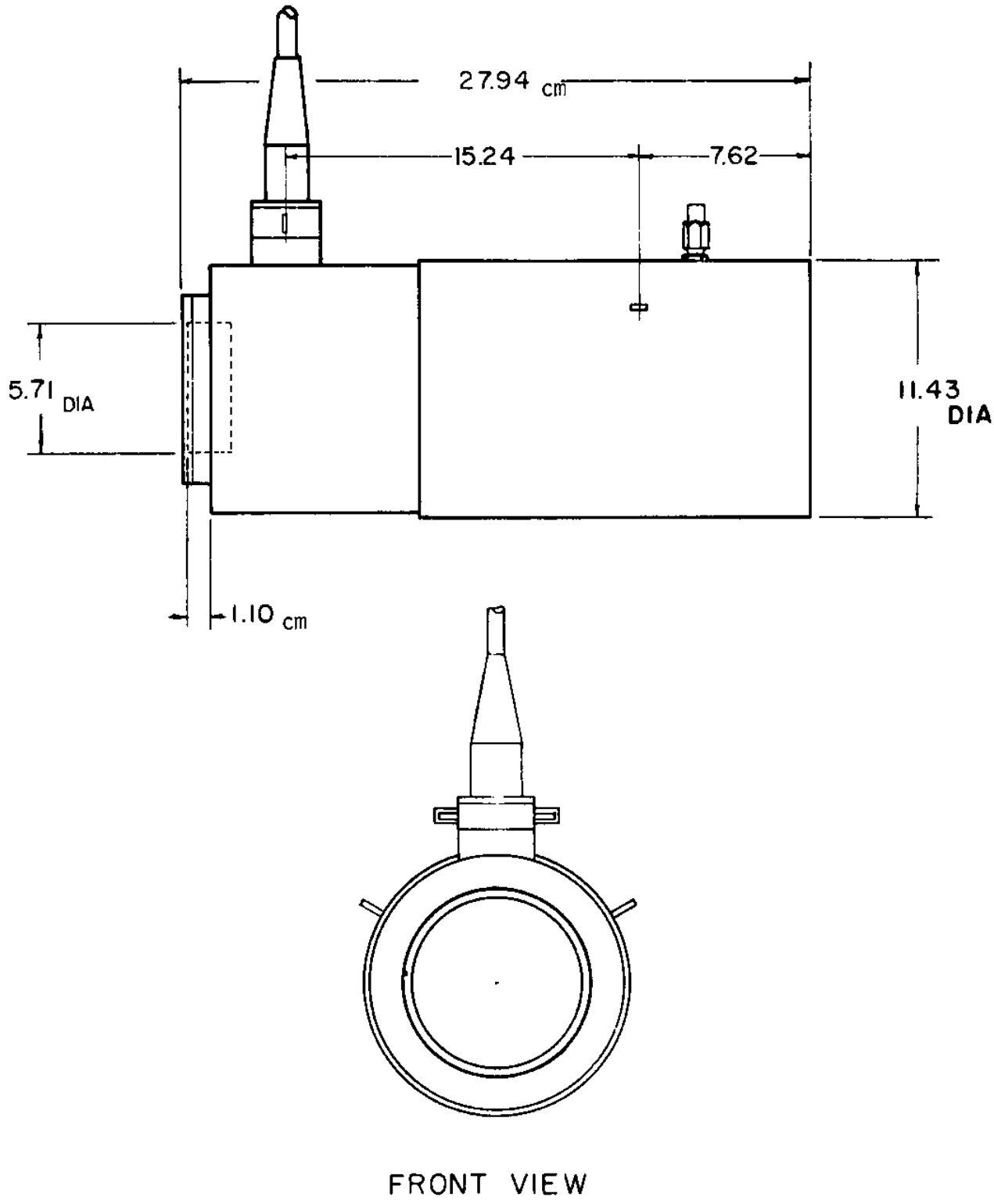

FIG. 22. Dimensions of type J9 transducer.

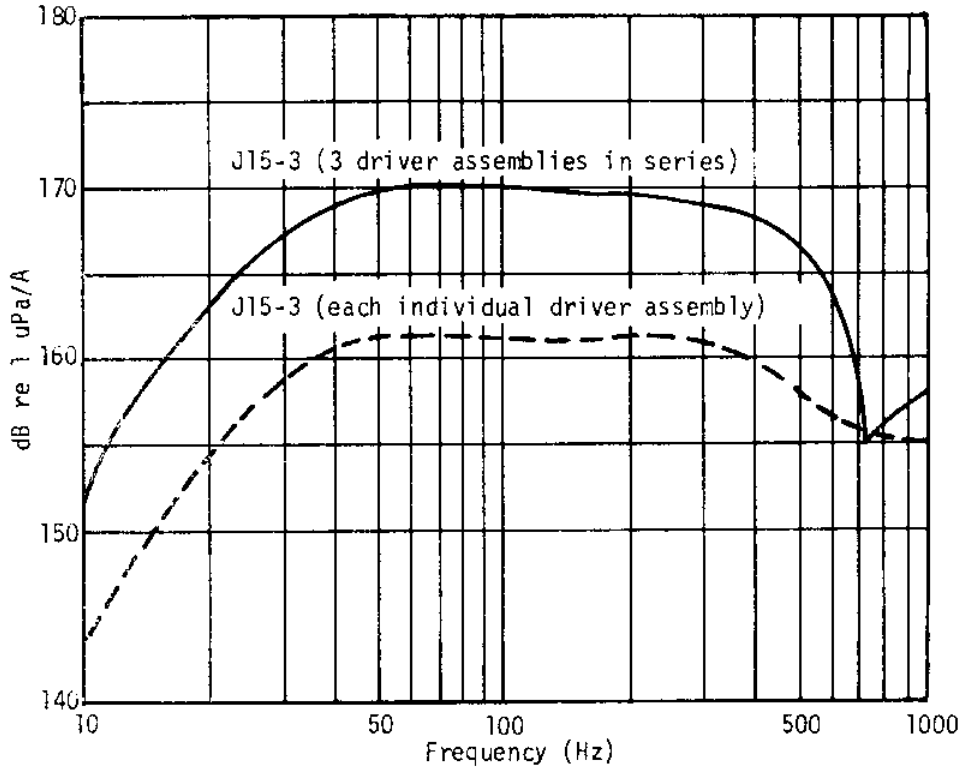

Fig.23. Typical transmitting current response, USRD type J15-3 transducer.

in Fig. 24.

Information about other standard hydrophones and transducers available from the NRL-USRD, Orlando, Florida, will be found in ref. 4.

Acknowledgments

I am indebted to my colleagues at the NRL-USRD for their permission to use the illustrations in the text. In particular I wish to thank R. J. Bobber for permission to draw generously from his book Underwater Electroacoustic Measurements.

References

1. R. J. Bobber, "Interference Versus Frequency in Measurements in a Shallow Lake," J. Acoust. Soc. Am. 33, 1211-1215 (1961).

2. R. J. Bobber, "Underwater Electroacoustic Measurements," U. S. Government Printing Office, Washington, D. C., July 1970.

3. I. D. Groves, Jr., "The Design of Deep-Submergence Hydrophones," NRL Report 7339, 3 Sep 1971 [AD-729643].

4. Scientific and Technical Services Available from the Underwater Sound Reference Division, Naval Research Laboratory, Services Schedule, 15 Nov 1972.

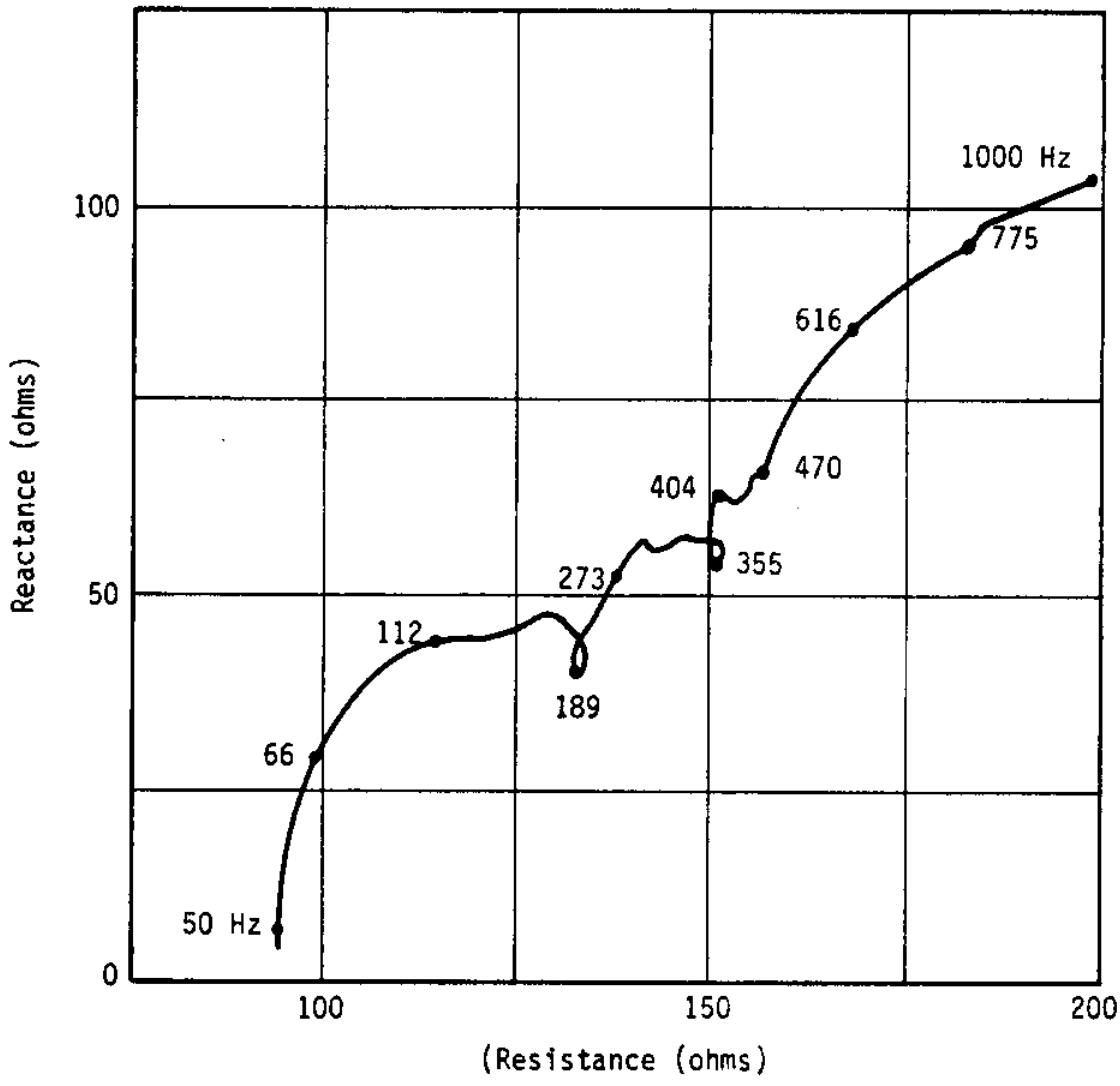

Fig. 24. Typical impedance, three driver assembly coils in series, USRD type J15-3 transducer.